Mass Spectrum of the Nucleon and Lambda in Lattice QCD

Derek Leinweber
CSSM Lattice Collaboration

Key Collaborators
Selim Mahbub, Ben Menadue, Dale Roberts,
Waseem Kamleh, Peter Moran and Tony Williams

Centre for the Subatomic Structure of Matter
School of Chemistry & Physics
University of Adelaide, SA, Australia

Outline

- Two point correlation function:

$$G_{ij}(t,\vec{p}) = \sum_{\vec{x}} e^{-i\vec{p}.\vec{x}} \langle \Omega | T\{\chi_i(x)\bar{\chi}_j(0)\} | \Omega \rangle .$$

- Inserting completeness

$$\sum_{B,\vec{p'},s} |B,\vec{p'},s\rangle\langle B,\vec{p'},s| = I$$

- Then

$$G_{ij}(t,\vec{p}) = \sum_{B^+} \lambda_{B^+}\bar{\lambda}_{B^+} e^{-E_{B^+}t} \frac{\gamma.p_{B^+} + M_{B^+}}{2E_{B^+}} + \sum_{B^-} \lambda_{B^-}\bar{\lambda}_{B^-} e^{-E_{B^-}t} \frac{\gamma.p_{B^-} - M_{B^-}}{2E_{B^-}}$$

- At $\vec{p} = 0$

$$\begin{aligned} G_{ij}^{\pm}(t,\vec{0}) &= \mathrm{Tr_{sp}}[\Gamma_{\pm} G_{ij}(t,\vec{0})] \\ &= \sum_{B^{\pm}} \lambda_i^{\pm} \bar{\lambda}_j^{\pm} e^{-M_{B^{\pm}} t}. \end{aligned}$$

- Parity projection operator,

$$\Gamma_{\pm} = \frac{1}{2}(1 \pm \gamma_0).$$

- Asymptotically

$$G_{ij}^{\pm}(t,\vec{0}) \overset{t \to \infty}{=} \lambda_{i0}^{\pm} \bar{\lambda}_{j0}^{\pm} e^{-M_{0^{\pm}} t}.$$

- In ensemble average, $G^{\pm}_{ij}(t) = G^{\pm}_{ji}(t)$
- $\frac{1}{2}[G^{\pm}_{ij}(t) + G^{\pm}_{ji}(t)]$ provides an improved unbiased estimator leads to use symmetric eigenvalue Eq.
- Effective mass, $M_{\mathrm{eff}}(t) = \ln\left(\frac{G(t)}{G(t+1)}\right)$

Interpolators

- Consider

$$\chi_1(x) = \epsilon^{abc}(u^{Ta}(x)\, C\gamma_5\, d^b(x))\, u^c(x)\,,$$
$$\chi_2(x) = \epsilon^{abc}(u^{Ta}(x)\, C\, d^b(x))\, \gamma_5\, u^c(x)\,,$$
$$\chi_4(x) = \epsilon^{abc}(u^{Ta}(x)\, C\gamma_5\gamma_4\, d^b(x))\, u^c(x).$$

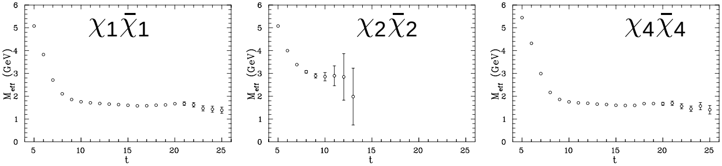

Variational Method

- Consider N interpolating fields, then

$$\bar{\phi}^{\alpha} = \sum_{i=1}^{N} u_i^{\alpha}\, \bar{\chi}_i\,,$$
$$\phi^{\alpha} = \sum_{i=1}^{N} v_i^{\alpha}\, \chi_i\,,$$

such that,

$$\langle B_\beta, p, s | \bar{\phi}^{\alpha} | \Omega \rangle = \delta_{\alpha\beta} \bar{z}^{\alpha} \bar{u}(\alpha, p, s),$$

$$\langle \Omega | \phi^{\alpha} | B_\beta, p, s \rangle = \delta_{\alpha\beta} z^{\alpha} u(\alpha, p, s),$$

- Then a two point correlation function matrix for $\vec{p} = 0$, right multiplied by u_j^α has the property

$$G_{ij}^{\pm}(t)\, u_j^\alpha = \Big(\sum_{\vec{x}} \mathrm{Tr}_{\mathrm{sp}}\{\Gamma_\pm \langle\Omega|\chi_i \bar{\chi}_j|\Omega\rangle\}\Big)\, u_j^\alpha$$
$$= \lambda_i^\alpha \bar{z}^\alpha e^{-m_\alpha t}.$$

(no sum over α)

- The t dependence is contained in the exponential term

- This provides a recurrence relation at time $(t_0 + \triangle t)$,

$$G_{ij}(t_0 + \triangle t)\, u_j^\alpha = e^{-m_\alpha \triangle t}\, G_{ij}(t_0)\, u_j^\alpha .$$

- Multiplying by $[G_{ij}(t_0)]^{-1}$ from left,

$$[(G(t_0))^{-1}\, G(t_0 + \triangle t)]_{ij}\, u_j^\alpha = c^\alpha\, u_i^\alpha ,$$

- where $c^\alpha = e^{-m_\alpha \triangle t}$ is the eigenvalue.
- Similarly, it can also be solved for the left eigenvalue equation for v^α eigenvector,

$$v_i^\alpha\, [G(t_0 + \triangle t)\, (G(t_0))^{-1}]_{ij} = c^\alpha\, v_j^\alpha .$$

- The vectors u_j^α and v_i^α diagonalize the correlation matrix at time t_0 and $t_0 + \triangle t$ making the projected correlation function

$$v_i^\alpha G_{ij}(t) u_j^\beta = \delta^{\alpha\beta} z^\alpha \bar{z}^\beta e^{-m_\alpha t}.$$

- The projected correlator, is then analyzed to obtain masses of different states,

$$v_i^\alpha G_{ij}^\pm(t) u_j^\alpha \equiv G_\pm^\alpha,$$

- Our effective mass is defined as

$$M_{\text{eff}}^\alpha(t) = \ln\left(\frac{G_\pm^\alpha(t,\vec{0})}{G_\pm^\alpha(t+1,\vec{0})}\right).$$

4×4 correlation matrix of χ_1 with 4 smearing levels

Projected Mass Vs Mass From Eigenvalue

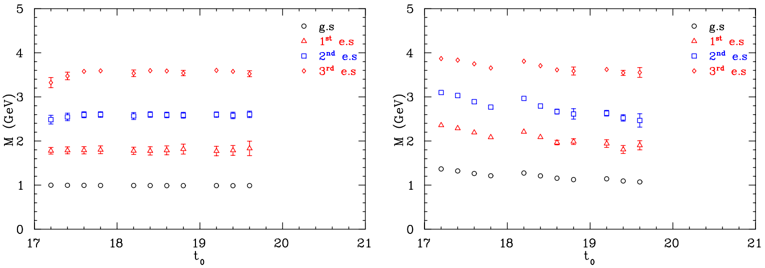

- t_0 is shown in major tick marks
- $\triangle t$ is shown in minor tick marks

PACS-CS Simulation Details

PACS-CS Collaboration: S. Aoki, et al., Phys. Rev. **D79** (2009) 034503.

- Lattice volume: $32^3 \times 64$
- Non-perturbative $\mathcal{O}(a)$-improved Wilson quark action
- Iwasaki gauge action
- $2 + 1$ flavour dynamical-fermion QCD
- $\beta = 1.9$ providing $a = 0.0907$ fm
- $K_{ud} = \{ 0.13700, 0.13727, 0.13754, 0.13770, 0.13781 \}$
- $K_s = 0.13640$
- Lightest pion mass is 156 MeV.
- Five ensembles of 350 configurations.
- 750 sources for lightest mass.

Sommer Scale

- Lattice spacing is set via the force between static quarks

$$r_c^2 \left. \frac{\partial V(r)}{\partial r} \right|_{r=r_c} = c$$

- Sommer prefers $c = 1.65$, such that $r_c = r_0 = 0.49$ fm
- The Sommer scale facilitates comparisons with other results

Source Smearing

Correlation matrices are built from a variety of source and sink smearings.

$$\psi_i(x,t) = \sum_{x'} F(x,x')\psi_{i-1}(x',t),$$

where,

$$\begin{aligned} F(x,x') &= (1-\alpha)\delta_{x,x'} + \frac{\alpha}{6}\sum_{\mu=1}^{3}[U_\mu(x)\delta_{x',x+\hat{\mu}} \\ &\quad + U_\mu^\dagger(x-\hat{\mu})\delta_{x',x-\hat{\mu}}], \end{aligned}$$

Fixing $\alpha = 0.7$, the procedure is repeated $N_{\rm sm}$ times.

Smeared Source - Point Sink Effective Masses

For second lightest quark mass and 50 configurations

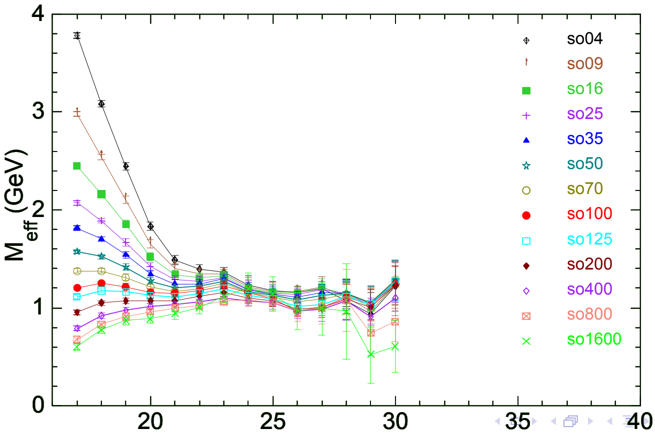

4×4 bases of $\chi_1 \bar{\chi}_1$

Sweeps $\rightarrow$	16	25	35	50	70	100	125	200	400	800
Basis No. $\downarrow$						Bases				
1	16	-	35	-	70	100	-	-	-	-
2	16	-	35	-	70	-	125	-	-	-
3	16	-	35	-	-	100	-	200	-	-
4	16	-	35	-	-	100	-	-	400	-
5	16	-	-	50	-	100	125	-	-	-
6	16	-	-	50	-	100	-	200	-	-
7	16	-	-	50	-	-	125	-	-	800
8	-	25	-	50	-	100	-	200	-	-
9	-	25	-	50	-	100	-	-	400	-
10	-	-	35	-	70	-	125	-	400	-

All 4 × 4 bases: second lightest mass

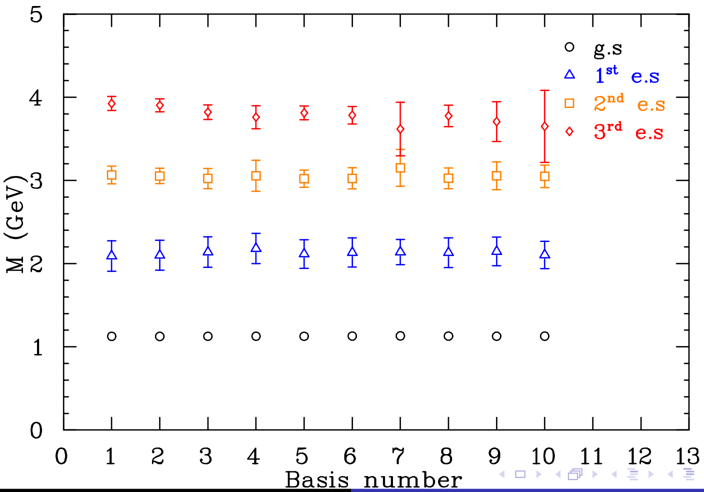

Even Parity Nucleon Spectrum in full QCD

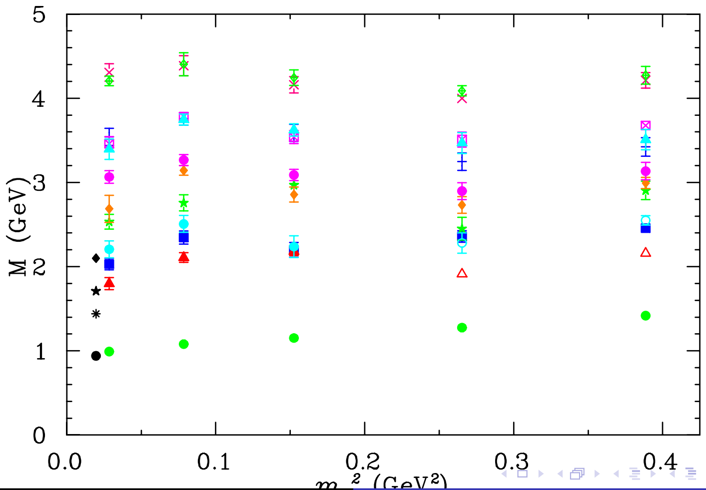

Even Parity Nucleon Spectrum in full QCD

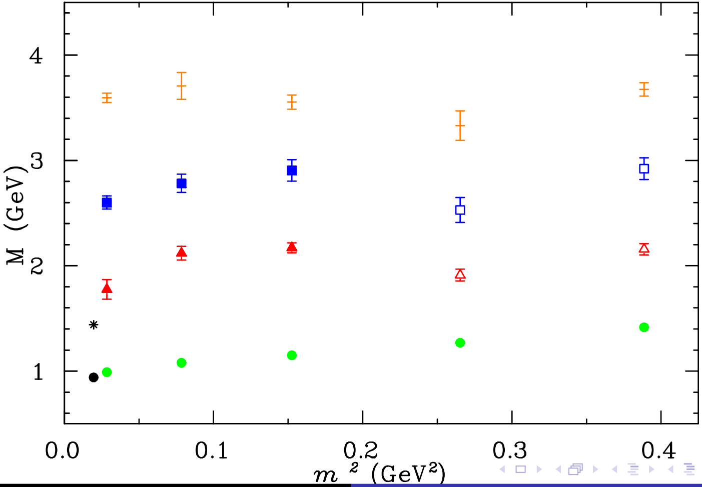

Even Parity Nucleon Spectrum in Quenched QCD

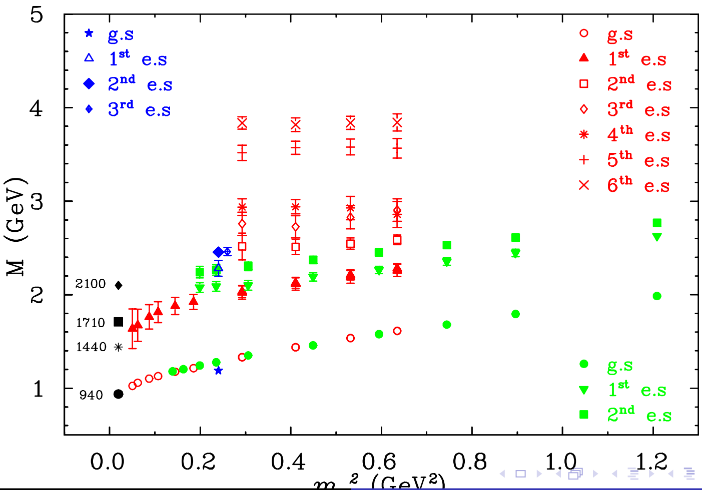

Even Parity Nucleon Spectrum in full QCD

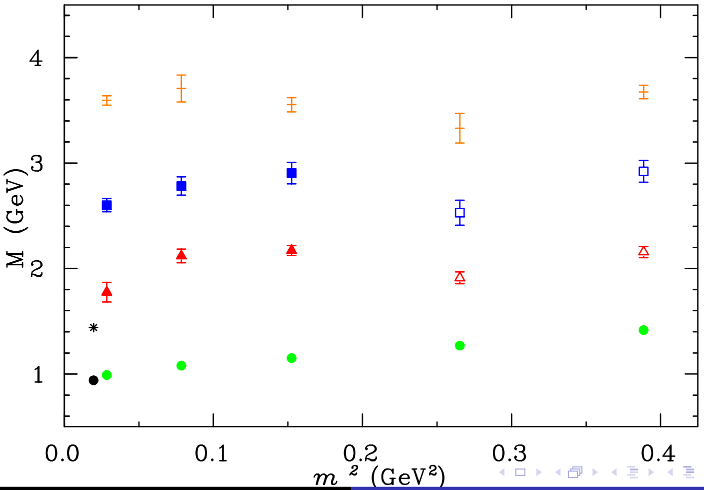

Even Parity Nucleon Spectrum in full QCD

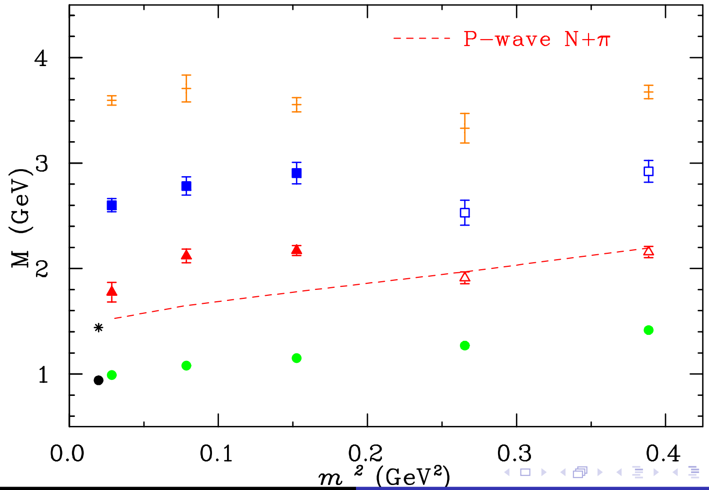

Even Parity Nucleon Spectrum in full QCD

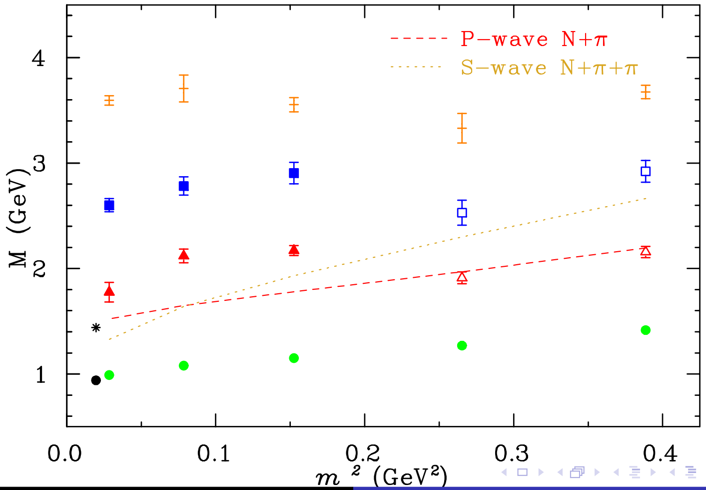

$N\frac{1}{2}^-$ (1535) State

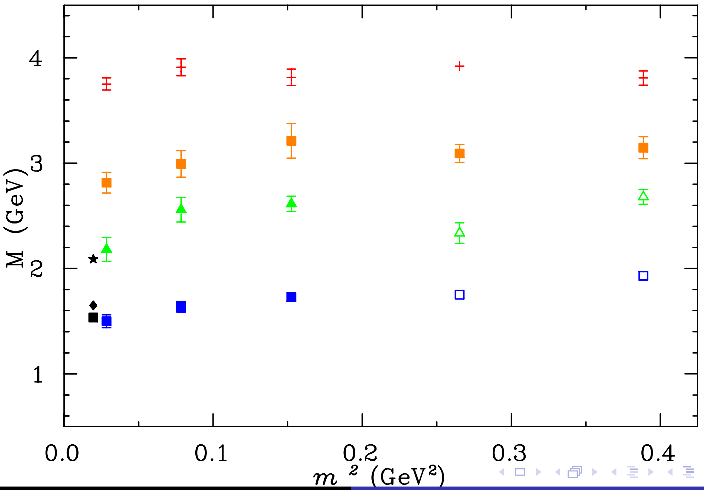

$N\frac{1}{2}^-$ (1535) State

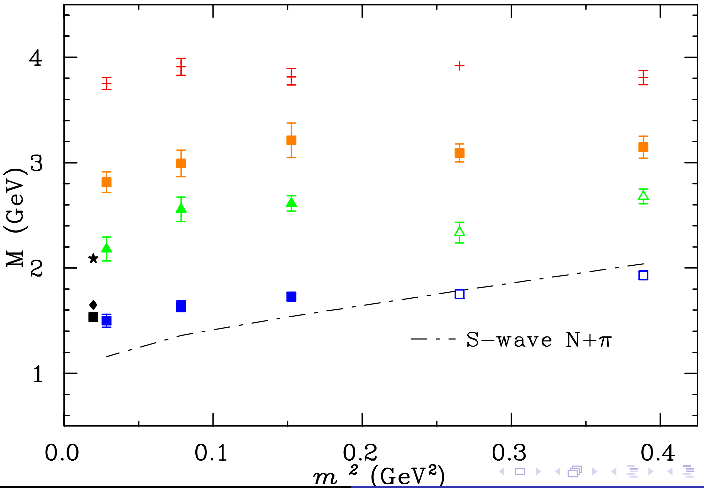

$N\frac{1}{2}^-$ (1535) State

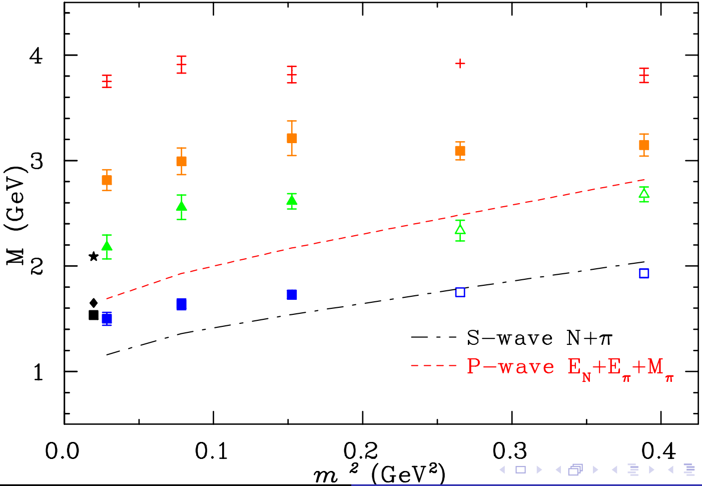

$N\frac{1}{2}^-$ (1535) State

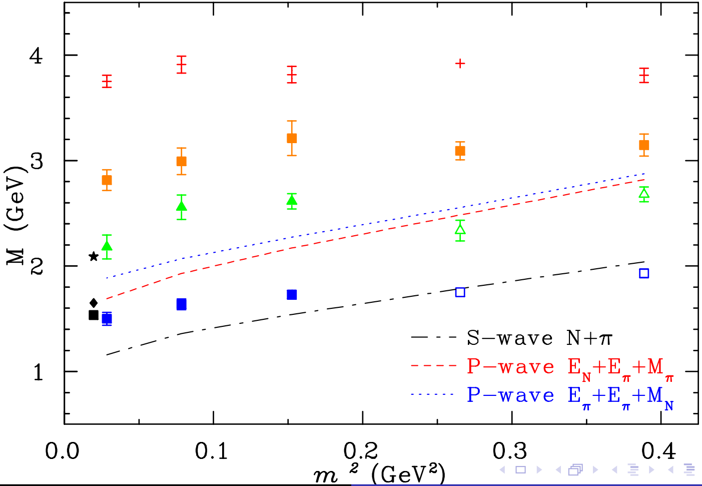

Loss of multi-particle states at light quark masses

Perhaps as the quark masses become light:

- Attractive spin-dependent forces, inversely related to quark masses, become strong.
- The generation of a resonance and its associated spectral strength masks the weakly-coupled scattering states.

On a finite volume lattice:

- The density of states increases with the lattice volume V.
- The coupling to the meson-baryon states is suppressed by $1/\sqrt{V}$.
- Therefore, scattering states are more difficult to excite on large volumes.

Quenched Vs Dynamical, N^+ states

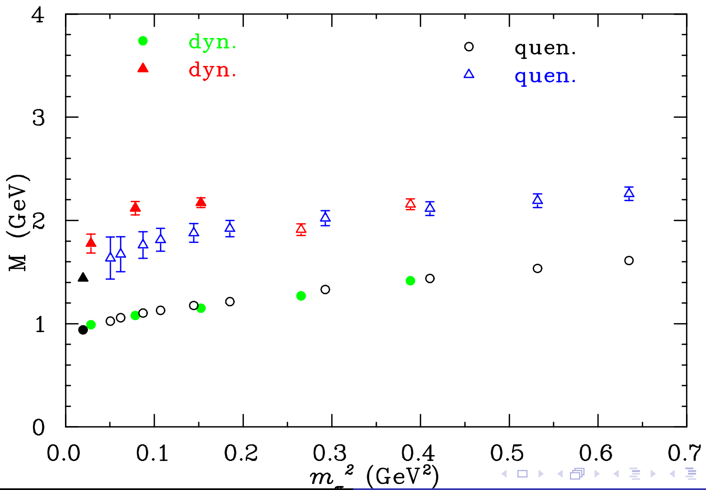

Quenched Vs Dynamical, N^+ states

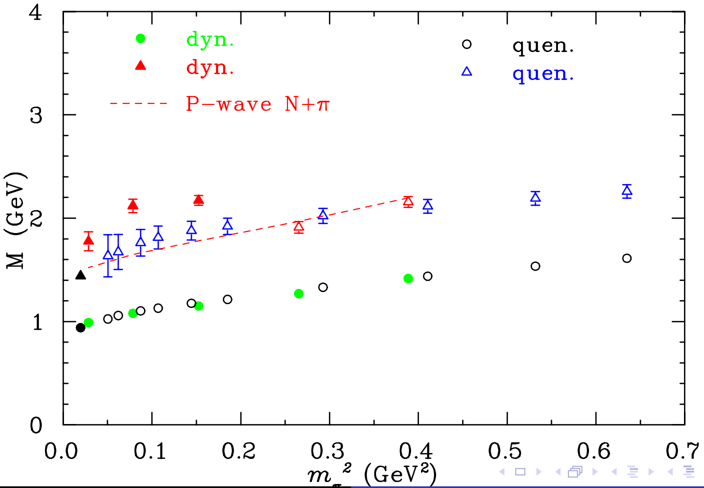

Quenched Vs Dynamical, N^+ states

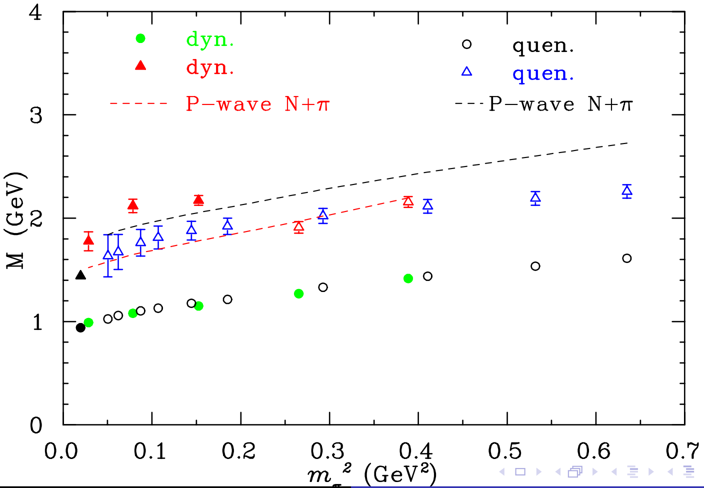

Quenched Vs Dynamical, N^- states

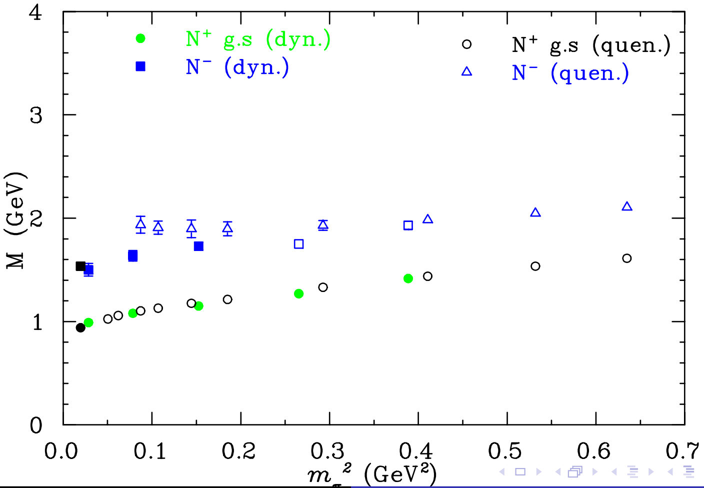

Quenched Vs Dynamical, N^- states

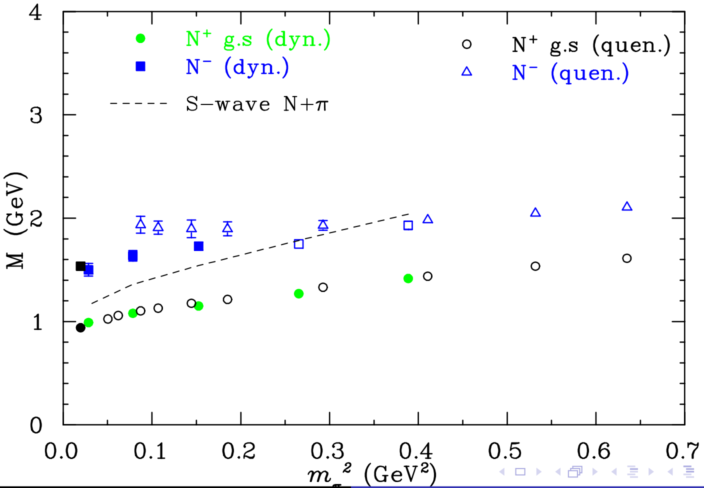

Quenched Vs Dynamical, N^- states

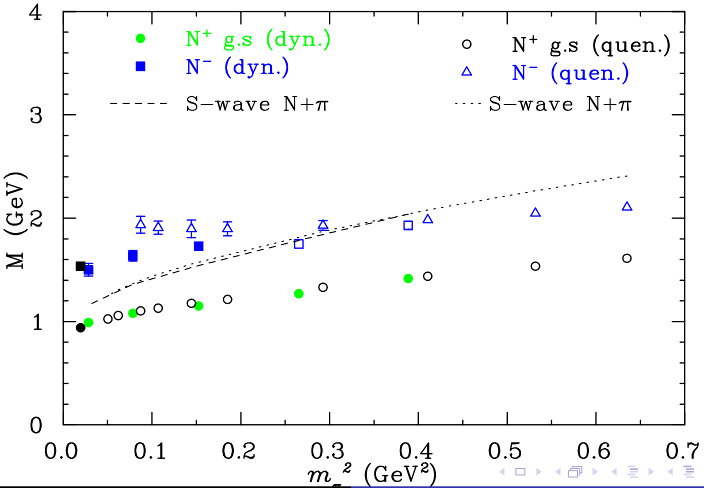

N^+ Spectrum for heaviest m_q: $4 \times 4 \rightarrow 8 \times 8$ $\chi_1 \chi_2$

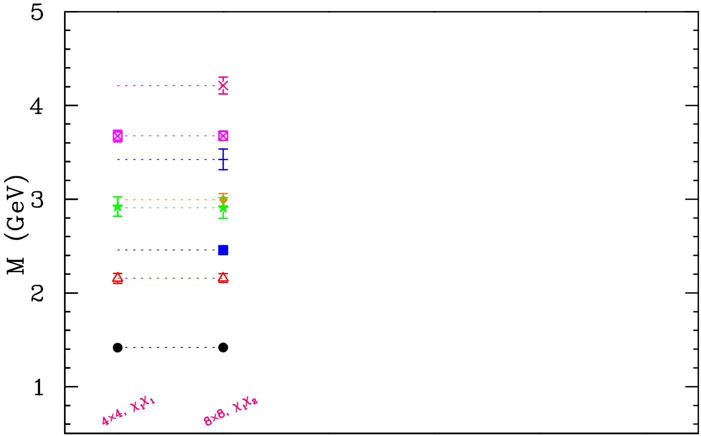

N^+ Spectrum for heaviest m_q: $8 \times 8\ \chi_2\,\chi_4$

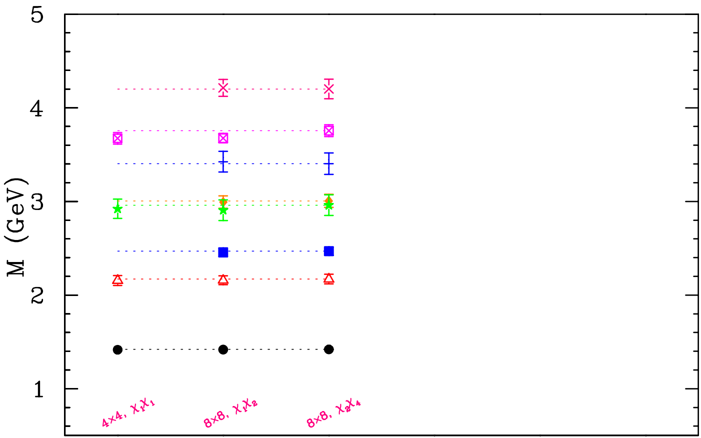

N^+ Spectrum for heaviest m_q: 8×8 $\chi_1 \chi_4$

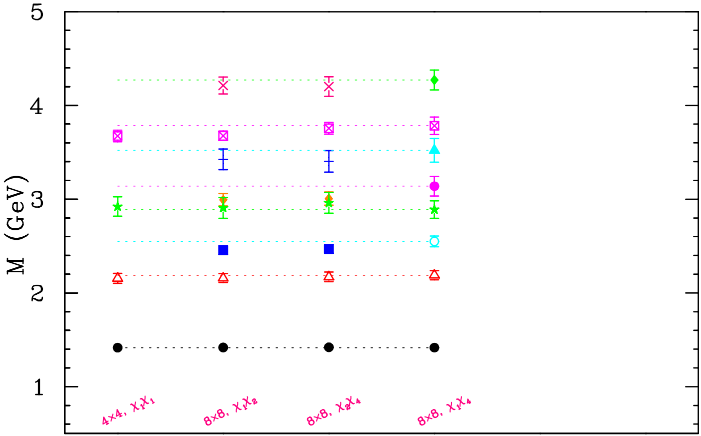

N^+ Spectrum for heaviest m_q: 12×12 $\chi_1\,\chi_2\,\chi_4$

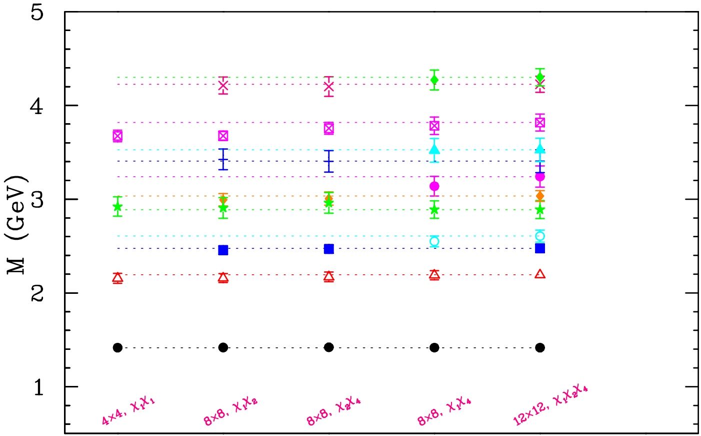

N^+ Spectrum for heaviest m_q: 8×8

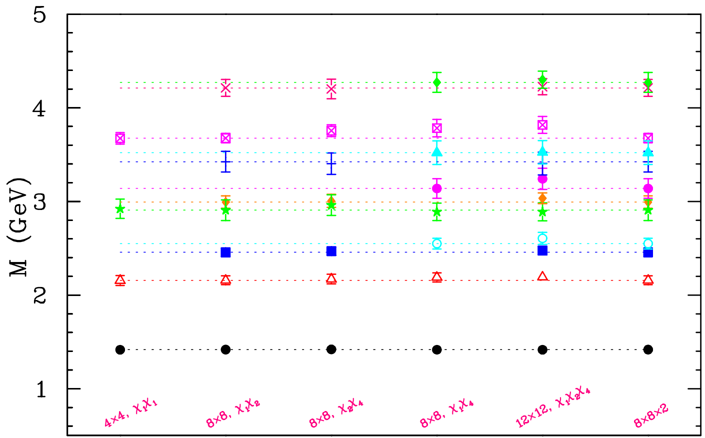

N^+ Spectrum: P-wave $N\,\pi$ threshold

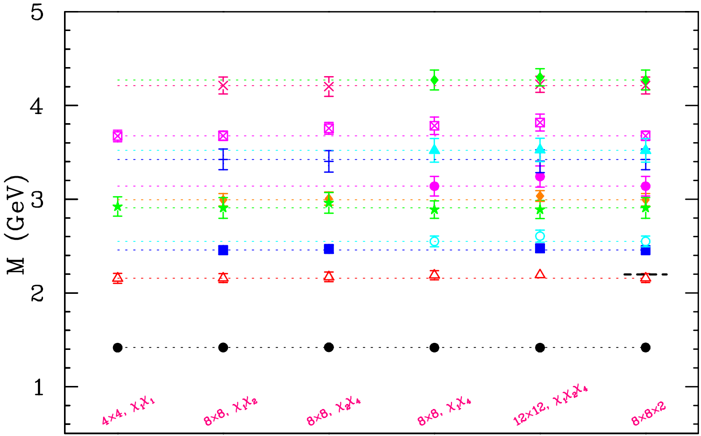

N^+ Spectrum: P-wave $N\pi$ and S-wave $N\pi\pi$

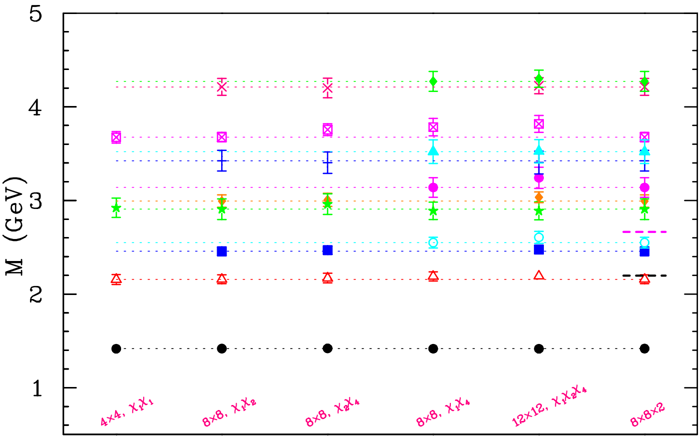

N^+ Spectrum for 2nd heaviest m_q: $4 \times 4 \to 8 \times 8$ $\chi_1\,\chi_2$

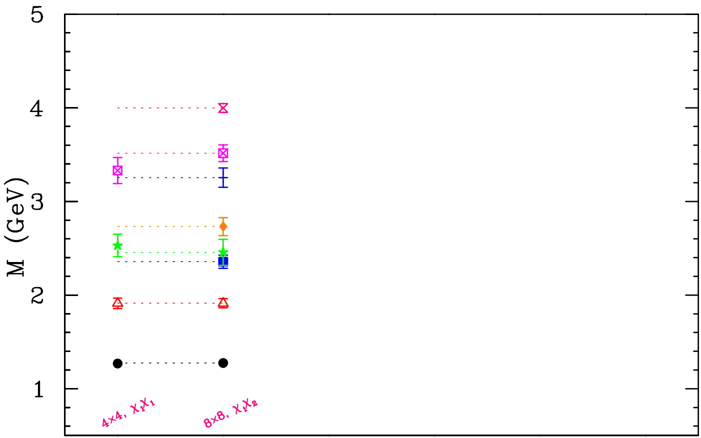

N^+ Spectrum for 2nd heaviest m_q: 8×8 $\chi_2\,\chi_4$

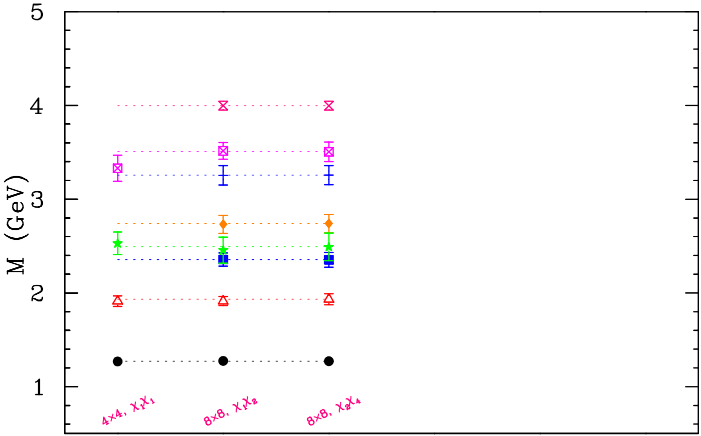

N^+ Spectrum for 2nd heaviest m_q: 8×8 $\chi_1\,\chi_4$

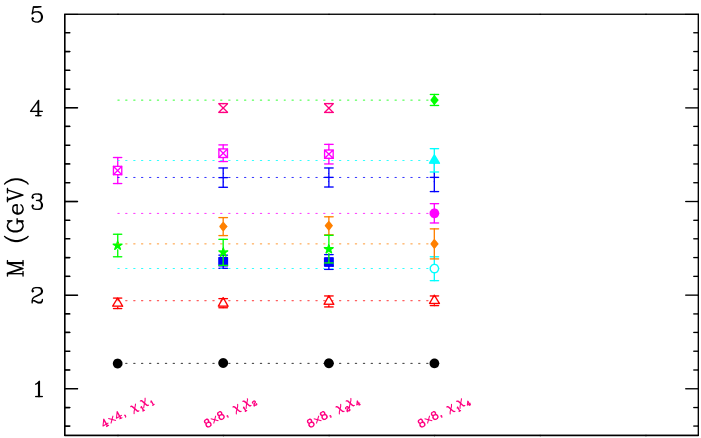

N^+ Spectrum for 2nd heaviest m_q: 8×8

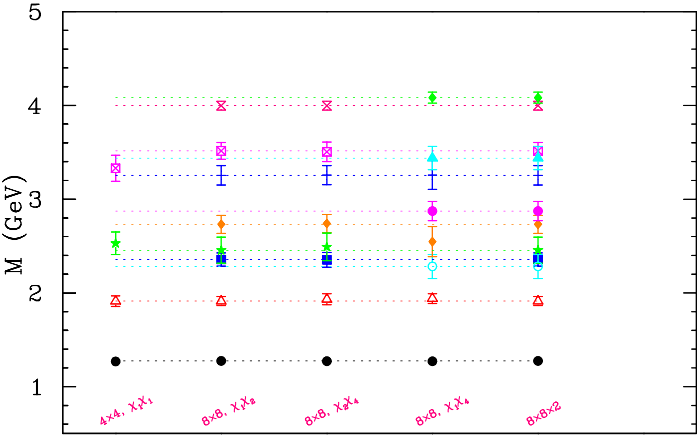

N^+ Spectrum for 2nd heaviest m_q: HSC Comparison

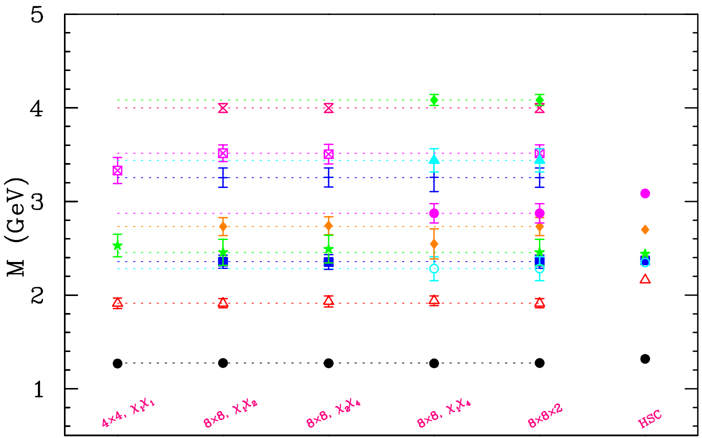

N^+ Spectrum for 2nd heaviest m_q: HSC Rescaled

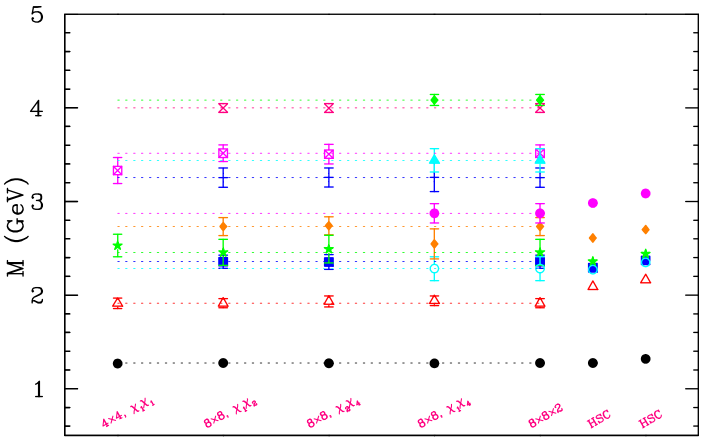

N^+ Spectrum: P-wave $N\,\pi$ thresholds

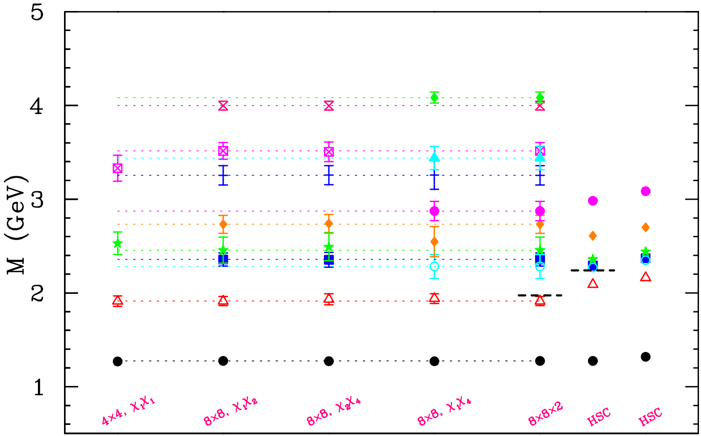

N^+ Spectrum: P-wave $N\,\pi$ and S-wave $N\,\pi\,\pi$

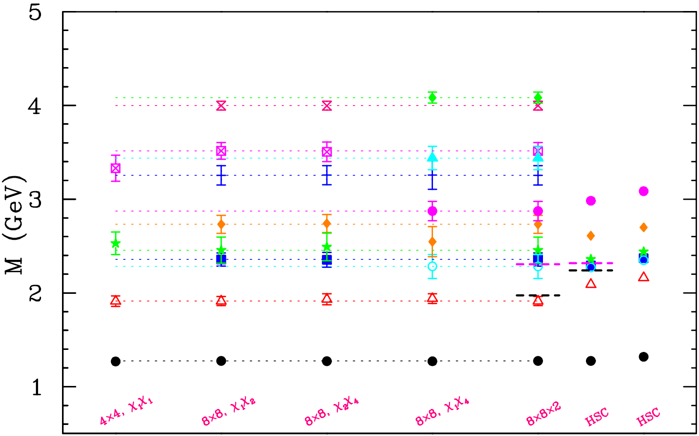

N^+ Spectrum for 3rd m_q: $4 \times 4 \rightarrow 8 \times 8$ $\chi_1 \chi_2$

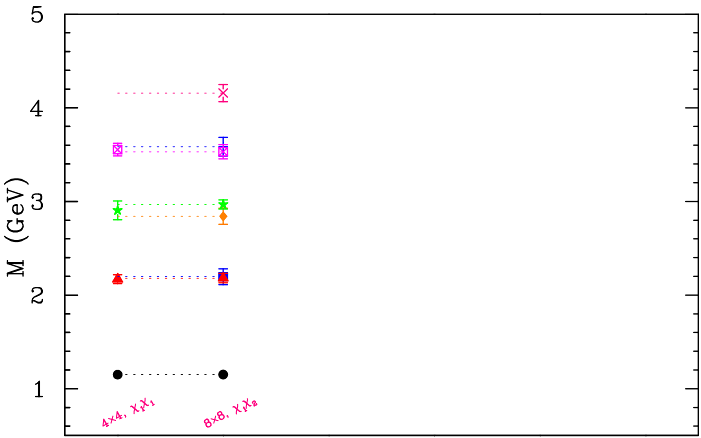

N^+ Spectrum for 3rd m_q: 8×8 $\chi_2\,\chi_4$

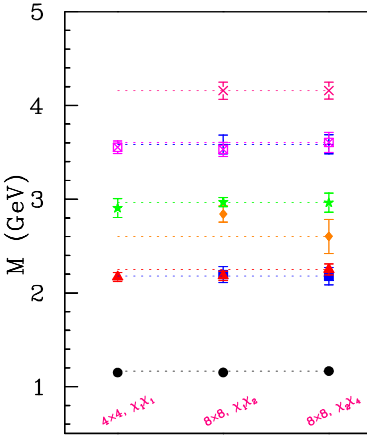

N^+ Spectrum for 3rd m_q: 8×8 $\chi_1\,\chi_4$

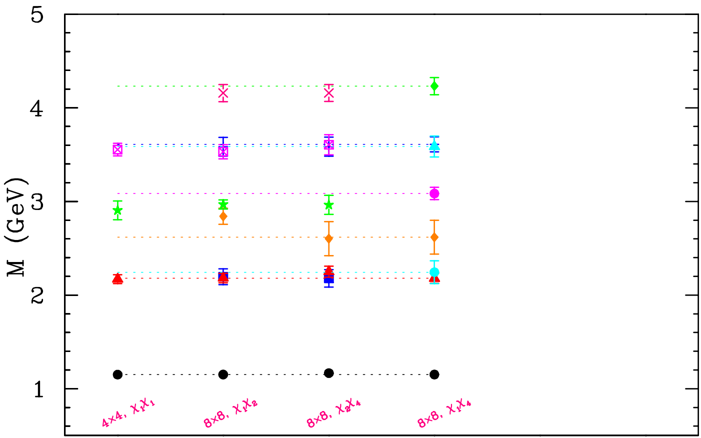

N^+ Spectrum for 3rd m_q: 8×8

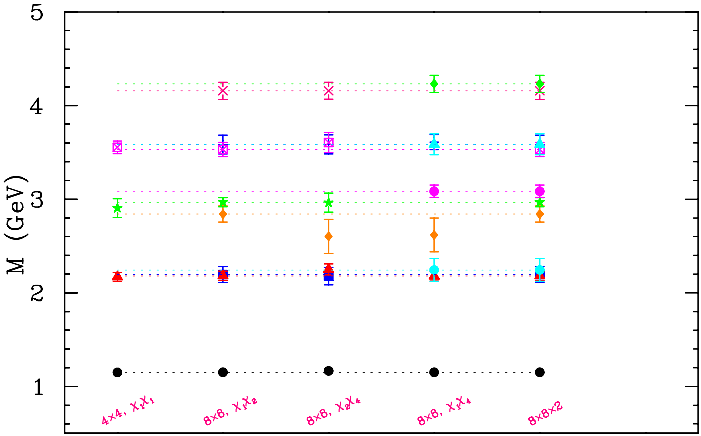

N^+ Spectrum for 3rd m_q: HSC Comparison

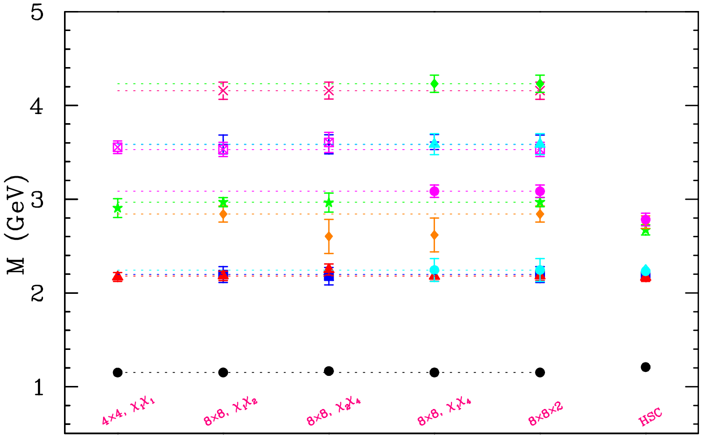

N^+ Spectrum for 3rd m_q: HSC Rescaled

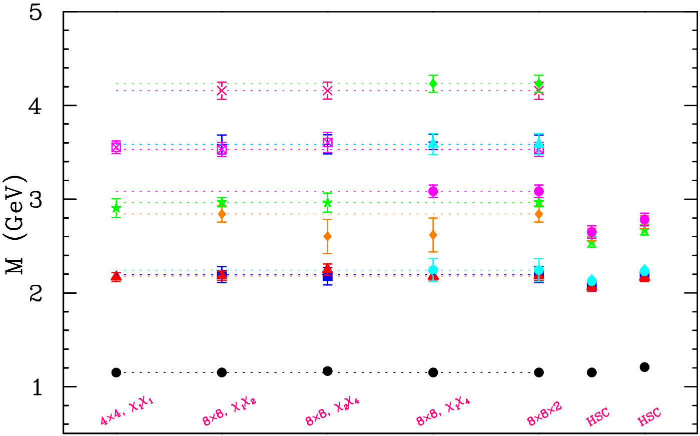

N^+ Spectrum: P-wave $N\,\pi$ thresholds

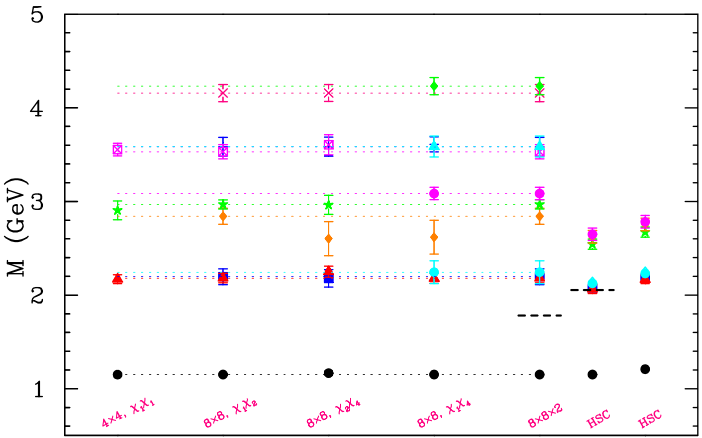

N^+ Spectrum: P-wave $N\pi$ and S-wave $N\pi\pi$

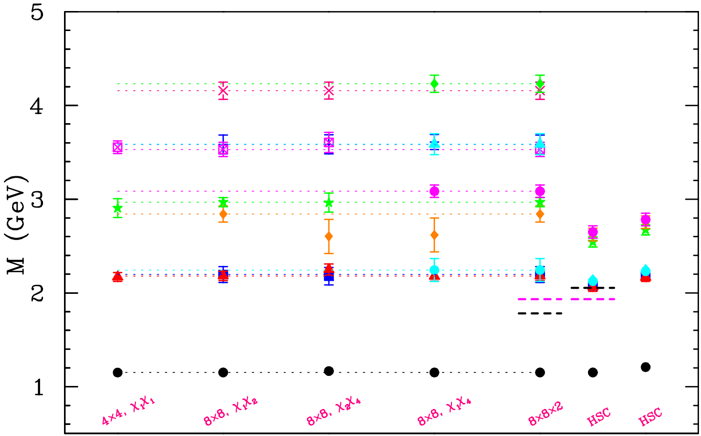

Quark-mass flow of eigenstates

- M interpolating fields making an $M \times M$ correlation matrix $G(t)$
- We determine $\vec{u}^{\alpha}$ of $[(G(t_0))^{-1} G(t_0 + \triangle t)]$
- Matrix $[(G(t_0))^{-1} G(t_0 + \triangle t)]$ is not symmetric. So $\vec{u}^{\alpha}$ are not orthogonal
- We explore the extent to which the eigenvectors $\vec{u}^{\alpha}(m_q)$ are orthogonal, by $\vec{u}^{\alpha}(m_q) \cdot \vec{u}^{\beta}(m_q)$
- By construction, $\vec{u}^{\alpha}(m_q) \cdot \vec{u}^{\beta}(m_q)$ is 1 for $\alpha = \beta$.

$\vec{u}^{\alpha}(m_q) \cdot \vec{u}^{\beta}(m_q)$

Table: The scalar product $\vec{u}^{\alpha}(m_q) \cdot \vec{u}^{\beta}(m_q)$ for $\kappa = 0.13700$, for 8×8 correlation matrix of χ_1 and χ_2.

$\alpha \downarrow$	$\beta \longrightarrow$						
1.00	0.02	-0.18	0.65	-0.07	0.10	-0.32	-0.09
0.02	**1.00**	0.02	0.07	0.15	0.06	0.42	0.03
-0.18	0.02	**1.00**	-0.10	0.36	-0.49	0.06	0.39
0.65	0.07	-0.10	**1.00**	-0.03	0.15	-0.57	-0.13
-0.07	0.15	0.36	-0.03	**1.00**	0.23	0.09	0.30
0.10	0.06	-0.49	0.15	0.23	**1.00**	-0.06	-0.61
-0.32	0.42	0.06	-0.57	0.09	-0.06	**1.00**	0.17
-0.09	0.03	0.39	-0.13	0.30	-0.61	0.17	**1.00**

Quark-mass flow of eigenstates continued · · ·

- This feature enables the use of the generalised measure

$$\mathcal{U}^{\alpha\beta}(m_q, m_{q'}) = \vec{u}^{\alpha}(m_q) \cdot \vec{u}^{\beta}(m_{q'})$$

- Can be used to identify the states most closely related as we move from quark mass m_q to adjacent quark mass $m_{q'}$.

$\mathcal{U}^{\alpha\beta}(m_q, m_{q'})$

Table: $\vec{u}^{\alpha}(m_q) \cdot \vec{u}^{\beta}(m_{q'})$, $\kappa = 0.13700$, $\kappa' = 0.13727$.

$\alpha \downarrow$	$\beta \longrightarrow$						
0.98	-0.29	-0.14	0.63	-0.07	0.10	-0.32	-0.08
-0.19	**-0.92**	0.08	-0.03	0.14	0.06	0.42	0.05
-0.16	0.07	**0.99**	-0.09	-0.04	-0.53	0.09	0.36
0.63	-0.44	-0.02	**0.99**	-0.05	0.13	-0.55	-0.12
-0.12	-0.11	0.40	0.00	**0.75**	0.00	0.08	0.36
0.05	-0.11	-0.42	0.17	0.76	**0.95**	-0.12	-0.53
-0.45	-0.17	0.03	-0.67	0.08	-0.05	**1.00**	0.18
-0.09	0.00	0.34	-0.14	-0.34	-0.82	0.21	**1.00**

Symmetric Correlation Matrix

- Recall, $G^{-1}(t_0)\, G(t_0 + \triangle t)\, |u_i\,\rangle \;=\; \lambda_i\, |u_i\,\rangle$
- Also, $G^{-1/2}(t_0)\, G^{+1/2}(t_0) \;=\; I$
- So, $G^{-1}(t_0)\, G(t_0 + \triangle t)\, G^{-1/2}(t_0)\, G^{+1/2}(t_0)\, |\, u_i\,\rangle \;=\; \lambda_i\, |u_i\,\rangle$
- Multiplying from the left by $G^{+1/2}(t_0)$ provides

$$G^{-1/2}(t_0)G(t_0 + \triangle t)G^{-1/2}(t_0)G^{+1/2}(t_0) \quad |u_i\rangle = \lambda_i G^{+1/2}(t_0) \quad |u_i\rangle$$

$$G^{-1/2}(t_0)G(t_0 + \triangle t)G^{-1/2}(t_0) \quad |w_i\rangle = \lambda_i \quad |w_i\rangle$$

where, $|w_i\rangle = G^{+1/2}(t_0)\, |u_i\,\rangle$

Symmetric Correlation Matrix

- $[G^{-1/2}(t_0)\, G(t_0 + \triangle t)\, G^{-1/2}(t_0)]$ is a real symmetric matrix with the same eigenvalue λ_i as before
- $\vec{w}^{\alpha}$ are orthogonal
- As in before, a scalar product of

$$\mathcal{W}^{\alpha\beta}(m_q, m_{q'}) = \vec{w}^{\alpha}(m_q) \cdot \vec{w}^{\beta}(m_{q'})$$

is constructed.

$\vec{w}^{\alpha}(m_q) \cdot \vec{w}^{\beta}(m_q)$

Table: $\vec{w}^{\alpha}(m_q) \cdot \vec{w}^{\beta}(m_q)$ for $\kappa = 0.13700$ and for an 8×8 "symmetric" correlation matrix of χ_1 and χ_2.

$\alpha \downarrow$	$\beta \longrightarrow$						
1.00	0.00	0.00	0.00	0.00	0.00	0.00	0.00
0.00	**1.00**	0.00	0.00	0.00	0.00	0.00	0.00
0.00	0.00	**1.00**	0.00	0.00	0.00	0.00	0.00
0.00	0.00	0.00	**1.00**	0.00	0.00	0.00	0.00
0.00	0.00	0.00	0.00	**1.00**	0.00	0.00	0.00
0.00	0.00	0.00	0.00	0.00	**1.00**	0.00	0.00
0.00	0.00	0.00	0.00	0.00	0.00	**1.00**	0.00
0.00	0.00	0.00	0.00	0.00	0.00	0.00	**1.00**

$\mathcal{W}^{\alpha\beta}(m_q, m_{q'})$

Table: $\vec{w}^{\alpha}(m_q) \cdot \vec{w}^{\beta}(m_{q'})$, $\kappa = 0.13700$, $\kappa' = 0.13727$.

$\alpha \downarrow$	$\beta \longrightarrow$						
1.00	-0.09	0.00	0.00	0.01	0.00	0.01	0.00
0.09	**0.99**	-0.07	0.13	-0.01	0.00	0.01	0.00
0.01	0.07	**1.00**	-0.01	0.00	-0.01	0.00	0.00
-0.01	-0.13	0.02	**0.98**	-0.09	0.02	0.07	0.00
0.01	0.01	0.00	-0.09	**-0.97**	0.21	-0.01	0.03
0.00	0.00	0.01	0.00	0.20	**0.95**	-0.07	-0.23
-0.01	0.00	0.00	-0.07	0.01	0.07	**0.99**	-0.01
0.00	0.00	0.00	-0.01	-0.08	-0.21	0.01	**-0.97**

$\mathcal{U}^{\alpha\beta}(m_q, m_{q'})$

Table: $\vec{u}^{\alpha}(m_q) \cdot \vec{u}^{\beta}(m_{q'})$, $\kappa = 0.13700$, $\kappa' = 0.13727$.

$\alpha \downarrow$	$\beta \longrightarrow$						
0.98	-0.29	-0.14	0.63	-0.07	0.10	-0.32	-0.08
-0.19	**-0.92**	0.08	-0.03	0.14	0.06	0.42	0.05
-0.16	0.07	**0.99**	-0.09	-0.04	-0.53	0.09	0.36
0.63	-0.44	-0.02	**0.99**	-0.05	0.13	-0.55	-0.12
-0.12	-0.11	0.40	0.00	**0.75**	0.00	0.08	0.36
0.05	-0.11	-0.42	0.17	0.76	**0.95**	-0.12	-0.53
-0.45	-0.17	0.03	-0.67	0.08	-0.05	**1.00**	0.18
-0.09	0.00	0.34	-0.14	-0.34	-0.82	0.21	**1.00**

States identified by $\vec{w}^{\alpha}(m_q) \cdot \vec{w}^{\beta}(m_{q'})$

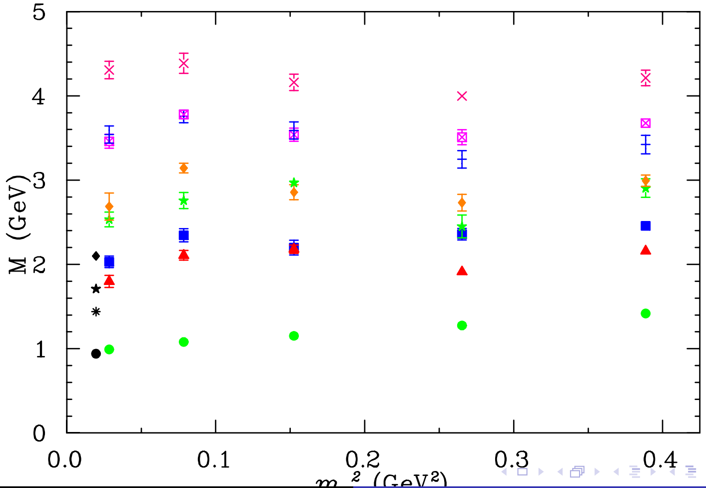

Eigenvectors, $|w_i\rangle$

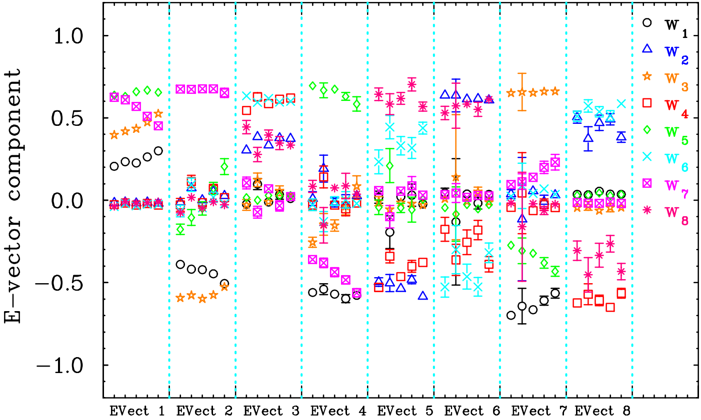

Eigenvectors, $|\, u_i \,\rangle \; = \; G^{-1/2}(t_0) \, |w_i\rangle$

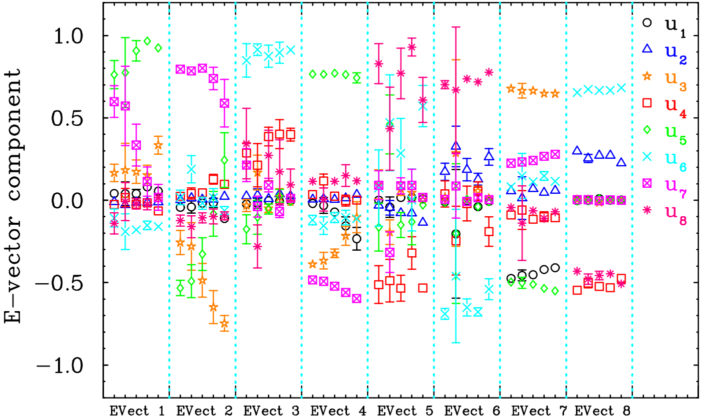

m_π^2 dependence of the N^+ Spectrum

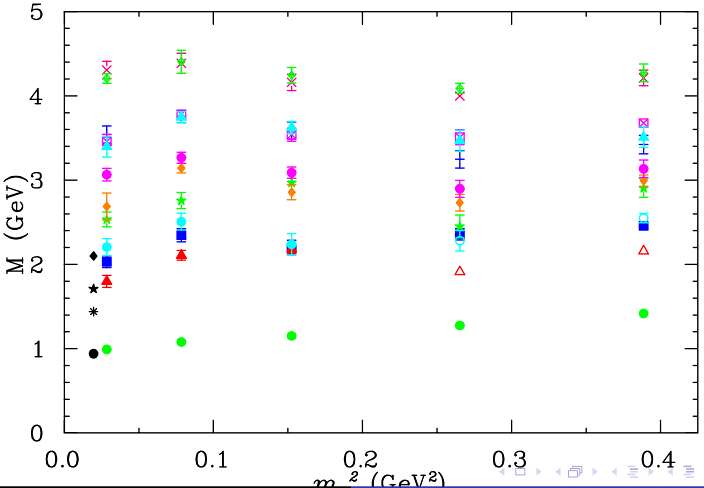

N^+ Spectrum: S and P-wave $N\,\pi$ thresholds

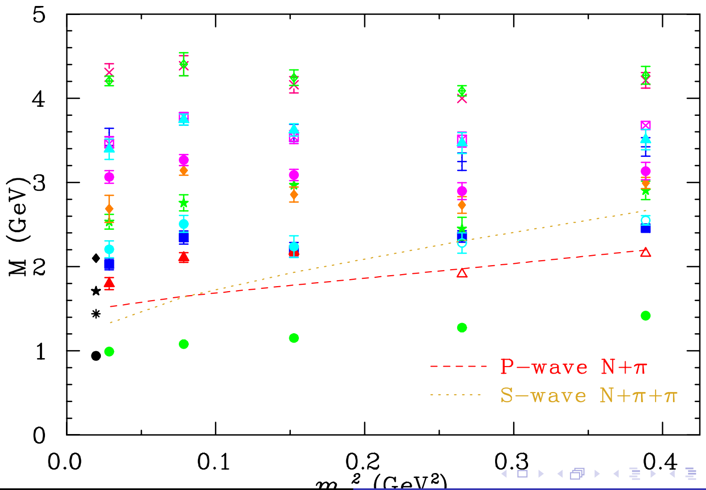

N^+ Spectrum: HSC Comparison

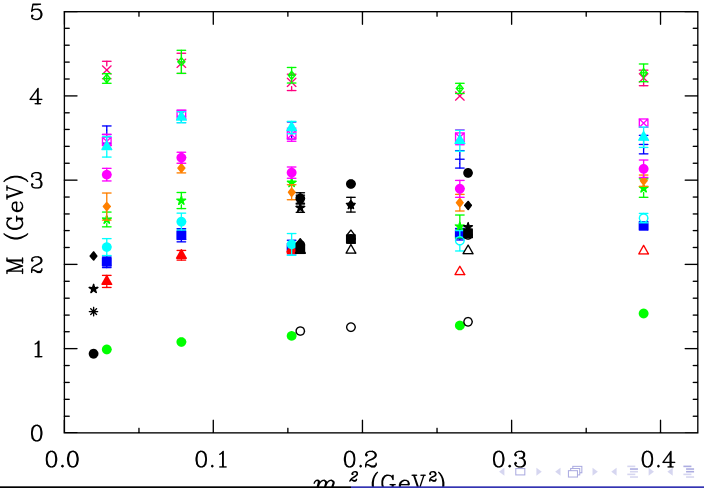

m_π^2 dependence of the $N\frac{1}{2}^-$ Spectrum

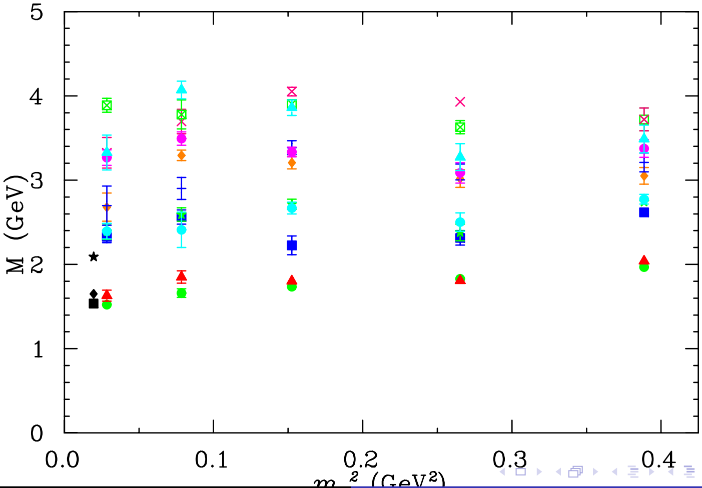

$N\frac{1}{2}^-$ Spectrum: S-wave $N\,\pi$ threshold

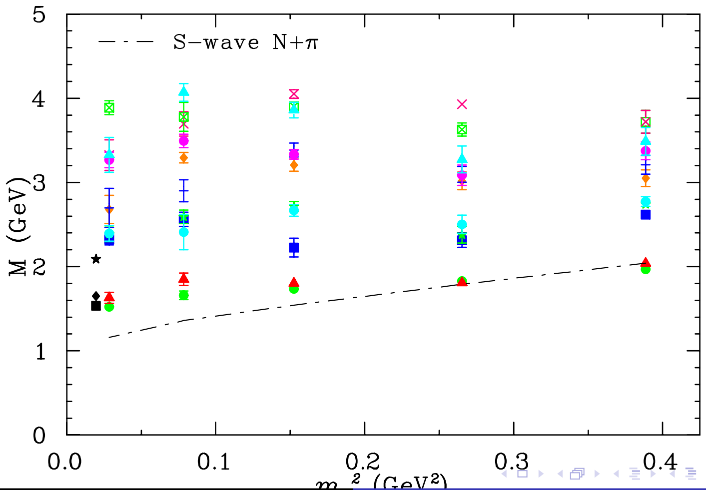

$N\frac{1}{2}^-$ Spectrum: S and P-wave $N\,\pi$ thresholds

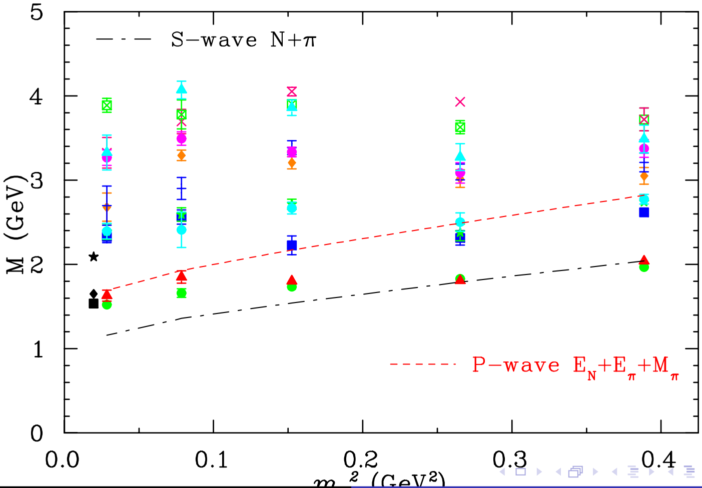

$N\frac{1}{2}^-$ Spectrum: S and P-wave $N\,\pi$ thresholds

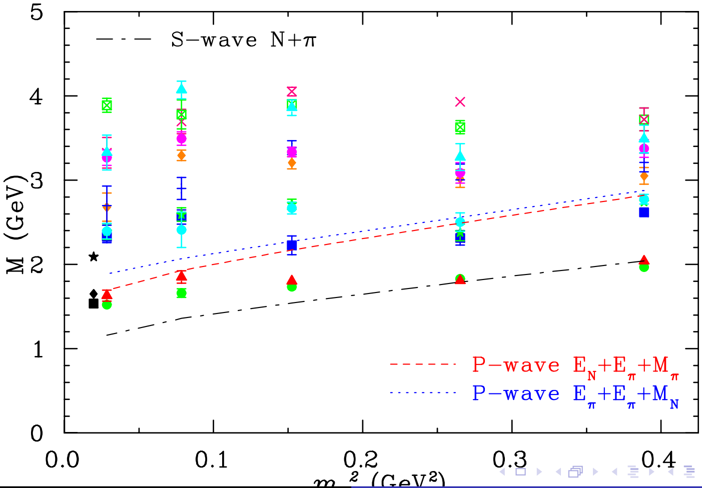

$N\frac{1}{2}^-$ Spectrum: with HSC [PRD84(2011)074508]

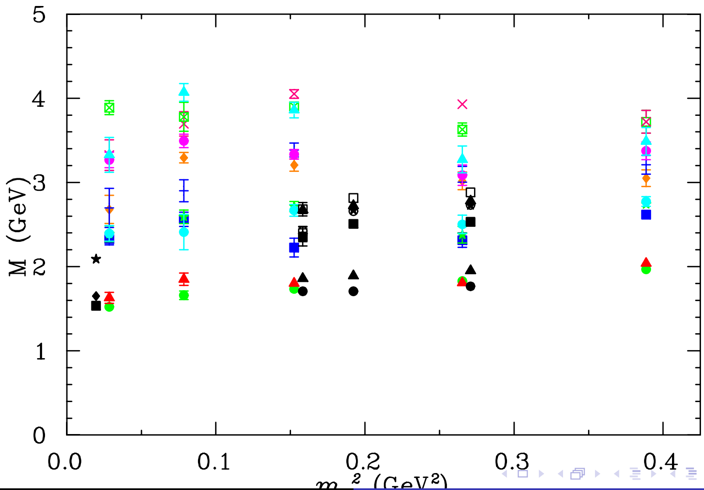

$N\frac{1}{2}^-$ Spectrum: with HSC [PRD84(2011)074508]

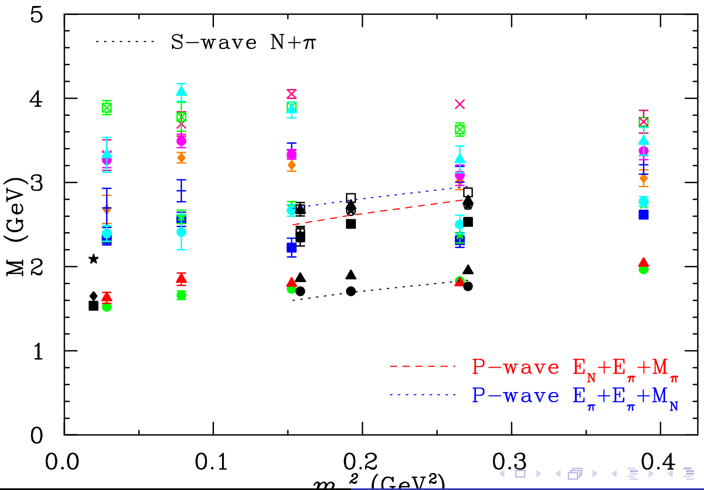

Wave functions from the lattice

- Generalize the baryon annihilation operator to

$$\epsilon^{abc}\left(u^{Ta}(\vec{x}+\vec{d},t)\,C\gamma_5\,d^b(\vec{x}+\vec{y},t)\right)\,u^c(\vec{x}-\vec{d},t)+$$
$$\epsilon^{abc}\left(u^{Ta}(\vec{x}-\vec{d},t)\,C\gamma_5\,d^b(\vec{x}+\vec{y},t)\right)\,u^c(\vec{x}+\vec{d},t)$$

  and measure the overlap of this operator with the state as a function of $\vec{y}$ for fixed $\vec{d}$.
- In this case, one obtains the wave function of the d quark.
- At the source, use $\bar{\phi}^\alpha=\sum_i u_i^\alpha\,\bar{\chi}_i$ to create the state α of interest.
- First consider $\vec{d}=0$; i.e. the distribution of the d quark about two u quarks at the origin.

Constituent Quark Model Wave Functions

- Consider a coulomb plus ramp potential with spin-dependent terms from

PHYSICAL REVIEW LETTERS

VOLUME 44 | 26 MAY 1980 | NUMBER 21

Quark-Quark Interaction and the Nonrelativistic Quark Model

R. K. Bhaduri, L. E. Cohler, and Y. Nogami
Department of Physics, McMaster University, Hamilton, Ontario L8S 4M1, Canada
(Received 14 January 1980; revised manuscript received 7 March 1980)

This Letter demonstrates that the nonrelativistic approximation breaks down for the lighter hadrons with the conventional qq one-gluon exchange potential. This is mainly due to the Coulomb and the short-range hyperfine interactions. To overcome this difficulty, some phenomenological interactions with a long-range spin dependence are proposed. The validity of treating the spin-dependent term as a perturbation is examined.

- Numerically solve SE on a periodic volume for the d quark

Ground-state wave function at lightest quark mass

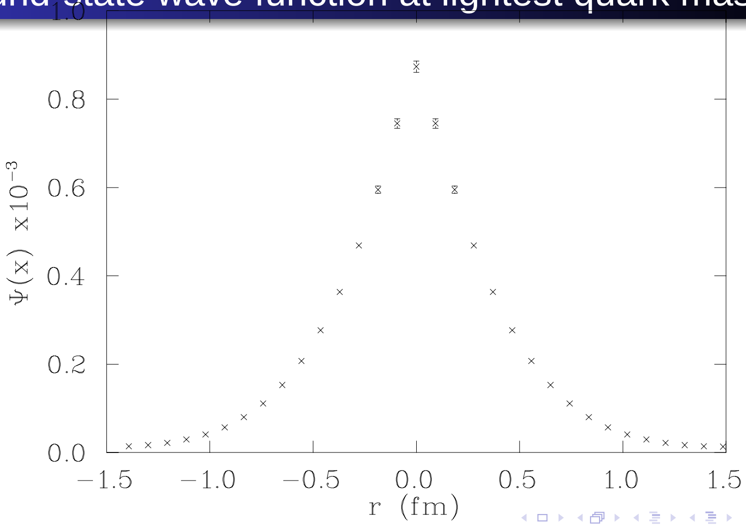

Roper wave function

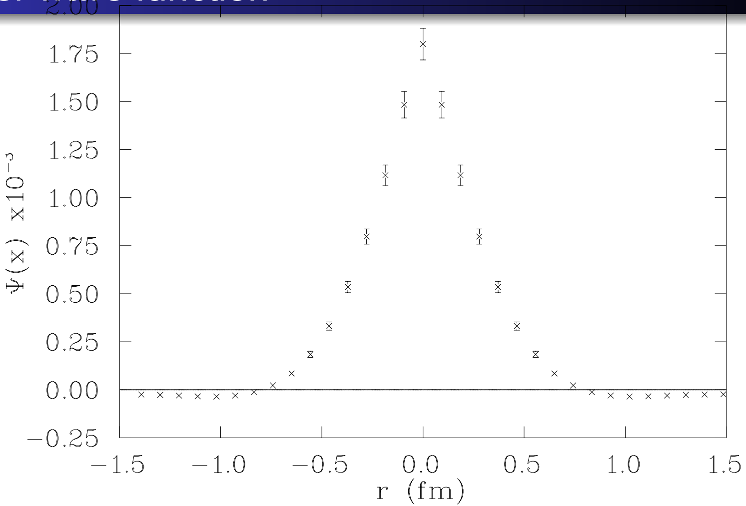

2nd excited-state wave function

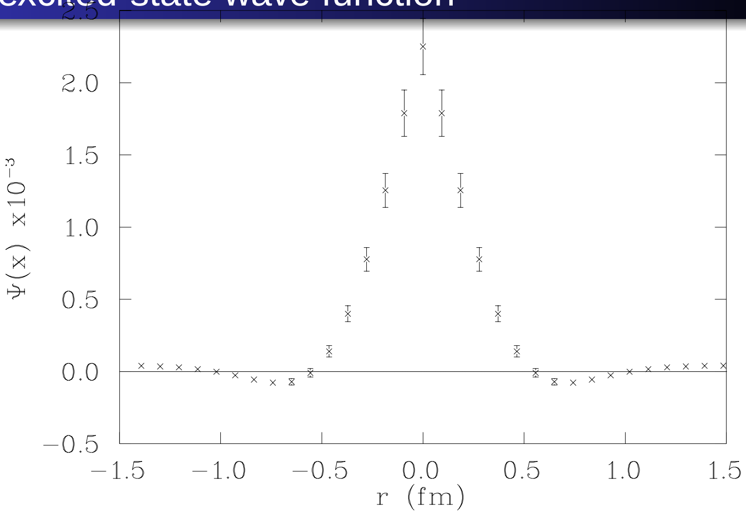

Ground-state density

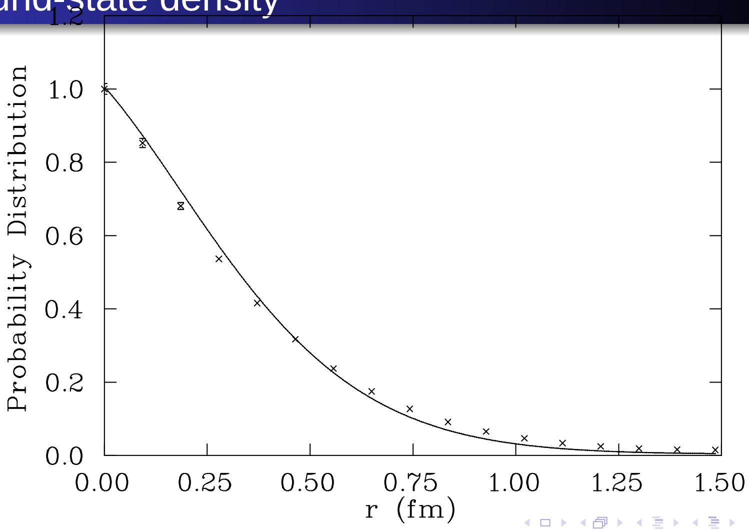

Roper density

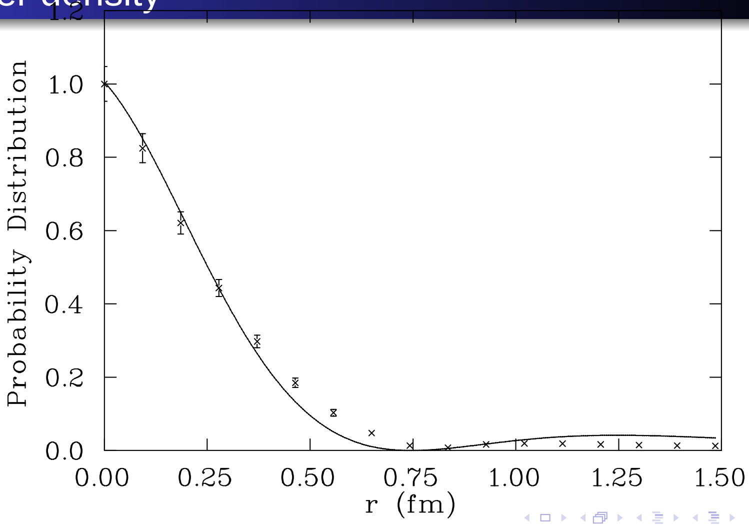

2nd excited-state density

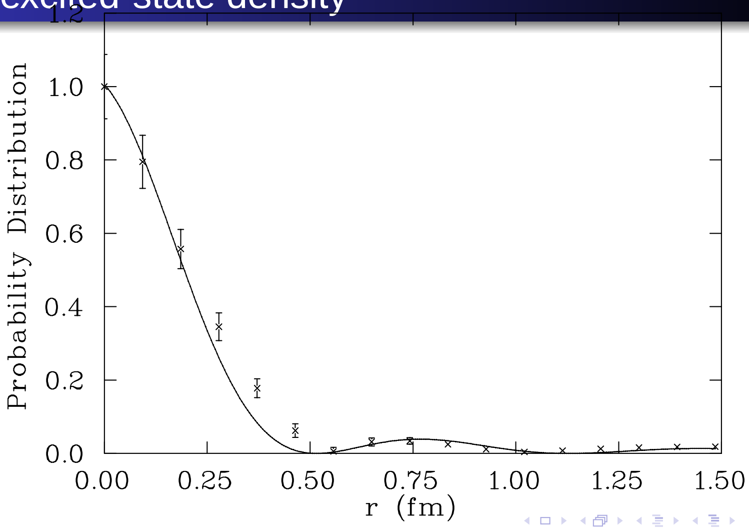

Ground-state density

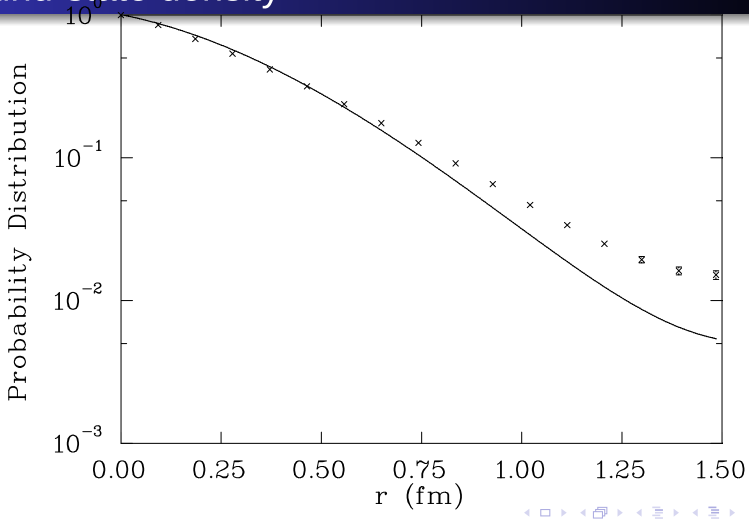

Roper density

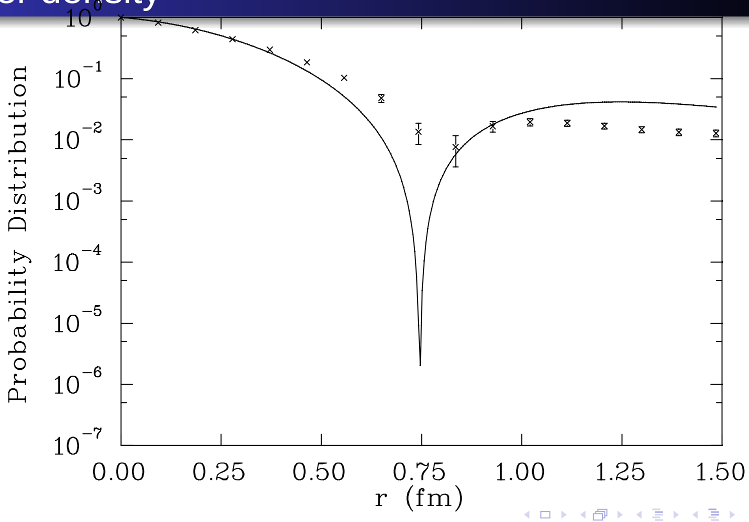

2nd excited-state density

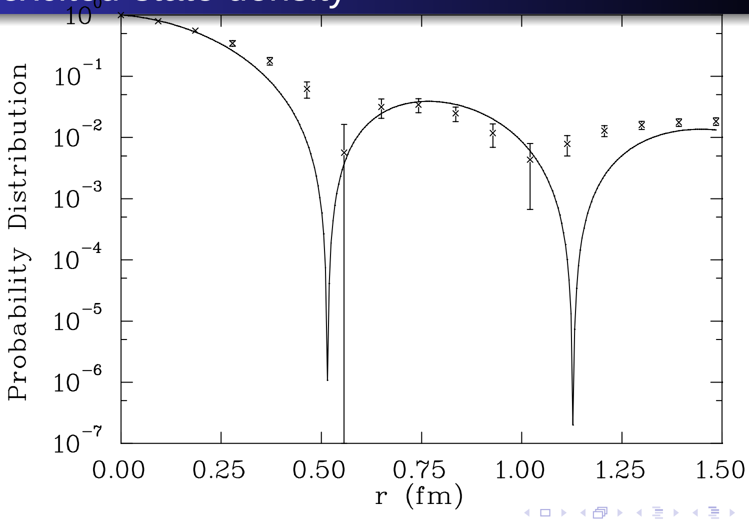

Finite Volume Effects

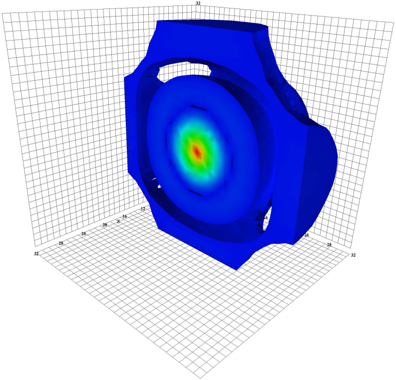

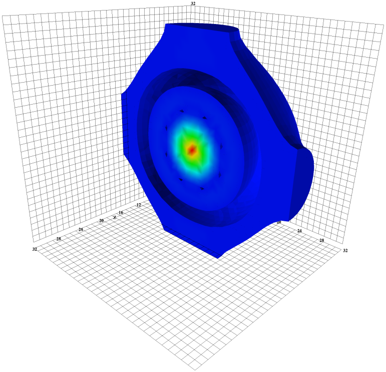

Projects

Nucleon Structure in the chiral regime

- m_π down to $\sim$ 160 MeV
- Nucleon EM form factors, $F_1(q^2)$, $F_2(q^2) \Rightarrow \langle r_1^2 \rangle$, $\langle r_2^2 \rangle$, μ `[arXiv:1106.3580]`
- Axial charge, $g_A \Rightarrow$ link to Nathan Hall `[arXiv:1206.7034]`
- Momentum fraction, $\langle x \rangle$
- Moments of Parton Distribution Functions and Generalised Parton Distribution Functions
- Glue in the Nucleon, e.g. $\langle x \rangle_g$ `[arXiv:1205.6410]`

Example: Isovector anomalous magnetic moment $\kappa^{(u-d)}$

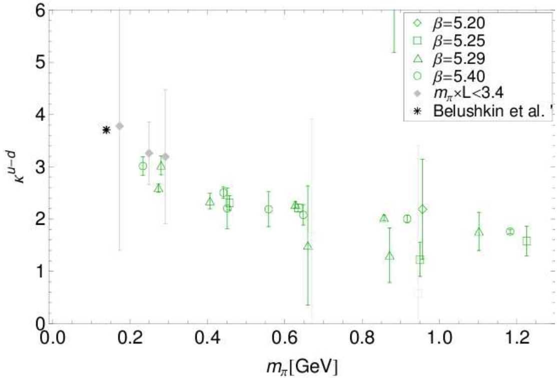

Projects

$SU(3)$-flavour breaking effects in hadrons

- Start from a world where u, d, s quarks have equal masses ($SU(3)_F$ symmetric limit)
- Monitor the dependence of hadronic observables on the quark mass splittings as they approach their physical values
  - Hadron spectrum [arXiv:1102.5300]
  - Sigma terms [arXiv:1110.4971] $\Rightarrow$ link to Phiala's work
  - Neutron-proton mass splitting [arXiv:1206.3156]
  - Charge symmetry violation in moments of nucleon PDFs (with Ross, Tony and Ian) [arXiv:1012.0215, 1204.3492]
  - Semi-leptonic Hyperon decays $\Rightarrow |V_{us}|$

Example: Octet Baryon Masses

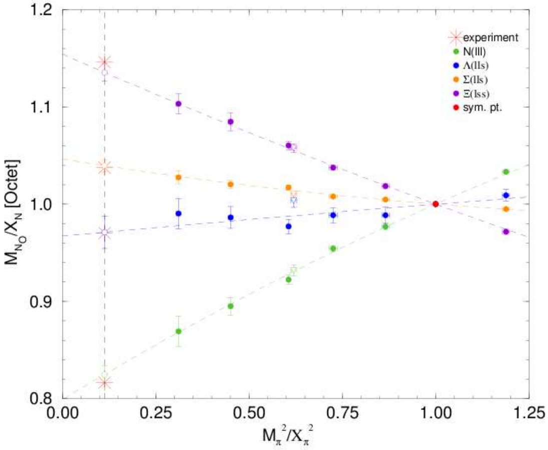

Chiral Effective Field Theory- Outline

- Using chiral effective field theory (χEFT), lattice QCD results can be extrapolated to the physical quark mass.
- Chiral loop integrals from χEFT contribute to nonanalytic curvature, which becomes significant for small pion masses ($m_q \propto m_\pi^2$).
- Using finite-range regularized (FRR) loop integrals, we introduce a regulator, $u(k\,;\Lambda)$, to cutoff the ultraviolet divergences in the momentum (k) integral.
- An optimal regularization scale, $\Lambda^{\rm scale}$, can be extracted from lattice QCD results.

Chiral Effective Field Theory- Outline

- The optimal scale can be used to perform reliable and robust chiral extrapolations.
- χEFT can also incorporate finite-volume corrections.
- For more details, see: *Power Counting Regime of Chiral Effective Field Theory and Beyond*, J.M.M. Hall, D.B. Leinweber (Adelaide U.), R.D. Young (Adelaide U. & Argonne). Feb 2010. 17 pp. Published in Phys.Rev. D82 (2010) 034010.

Magnetic Moment of the Nucleon

- The loop diagrams below are the leading-order contributions to the magnetic moment of the nucleon, μ.

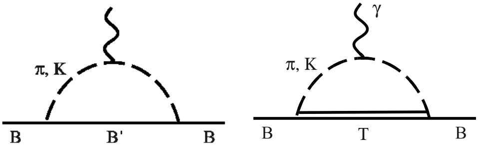

- In applying χEFT, we choose a dipole regulator to cutoff the divergences in the loop integrals:

$$u(k\,;\Lambda) = \left(1 + \frac{k^2}{\Lambda^2}\right)^{-2} . \tag{1}$$

Magnetic Moment of the Nucleon

- Chiral extrapolations of μ for several lattice sizes L:

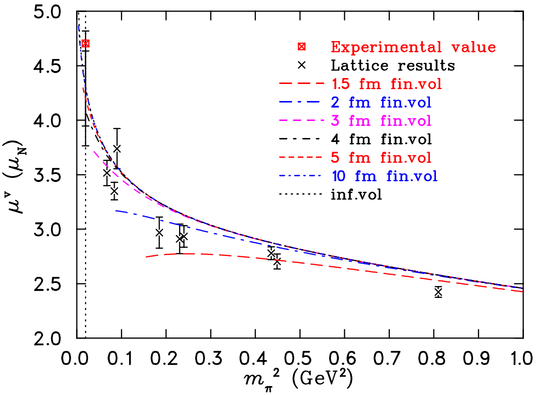

Magnetic Moment of the Nucleon

- Chiral extrapolations of μ (infinite-volume data):

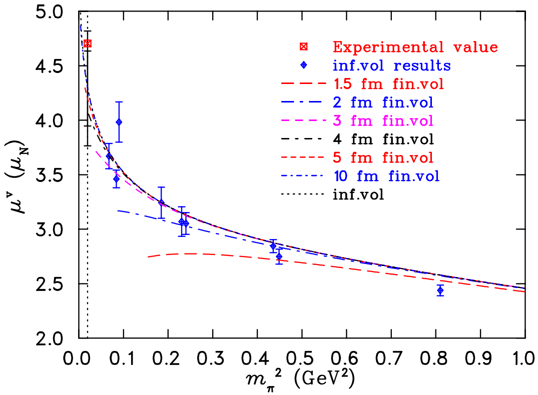

Electric Charge Radius of the Nucleon

- The χEFT loops shown below are the leading-order contributions to the electric charge radius of the nucleon, $\langle r^2 \rangle_E$.

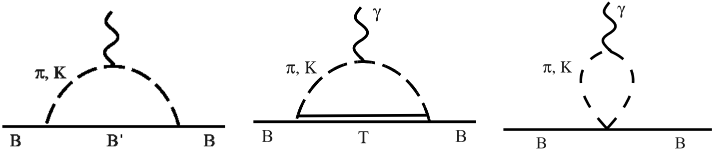

- A dipole regulator is again used in these integrals.

Electric Charge Radius of the Nucleon

- Chiral extrapolations of $\langle r^2 \rangle_E$ for several lattice sizes L:

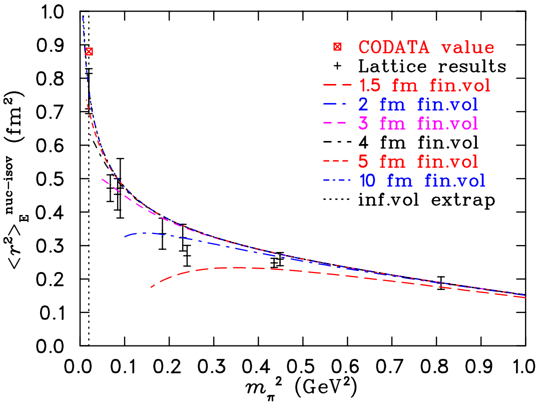

Electric Charge Radius of the Nucleon

- Chiral extrapolations of $\langle r^2 \rangle_E$, (infinite-volume data):

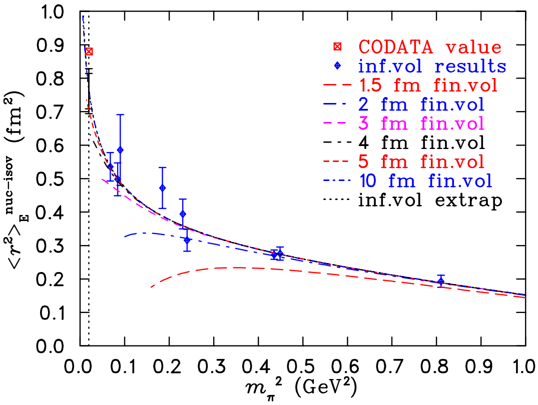

$\Delta N\pi$ Scattering

- For a nucleon and pion scattering off a Δ-baryon resonance, there is an associated phase shift δ.
- We can write out a t-matrix as a function of momentum k, or energy, $E = \sqrt{k^2 + m^2}$:

$$T = -\frac{1}{\pi k\, E}\, e^{i\delta(k)} \sin\delta(k). \tag{2}$$

- The t-matrix depends on χEFT, and receives inputs such as the coupling strength g, and the loop integral below:

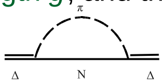

- We can plot δ as a function of energy E to get a Breit-Wigner type curve, with resonance at 90°.

Scattering Phase Shift

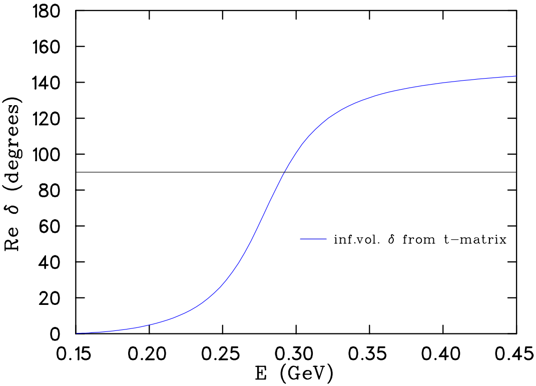

Figure: The phase shift associated with $N\pi$-scattering with a Δ-baryon intermediate, plotted against E, the external energy. $M_\Delta = M_N + E_{\text{res}}$.

Relating Finite-Volumes to Experiment

- It is important to find ways of relating finite-volume lattice calculations to experiment.
- One example is Lüscher's formula:

$$\delta(k\,;\,L) = r\,\pi - \phi(kL), \tag{3}$$

- which relates the momentum k, associated with an energy level, to the phase shift δ, through some known kinematic function ϕ.
- We can test Lüscher's formula with an exactly-solvable Hamiltonian model.

A $\Delta N\pi$ Hamiltonian Model

- Baryon resonances can be investigated in a finite volume, by constructing a matrix Hamiltonian model. For the $\Delta N\pi$, we have:

$$H = \begin{pmatrix} \Delta_0 & g_{\Delta N}(k_1) & g_{\Delta N}(k_2) & \cdots \\ g_{\Delta N}(k_1) & \sqrt{k_1^2 + m_\pi^2} & 0 & \cdots \\ g_{\Delta N}(k_2) & 0 & \sqrt{k_2^2 + m_\pi^2} & \cdots \\ \vdots & \vdots & \vdots & \ddots \end{pmatrix}, \tag{4}$$

- for a bare resonance energy Δ_0, and couplings $g_{\Delta N}(k)$ derived from χEFT.

Energy Levels from the Hamiltonian

- The ten lowest energy levels from the model. Non-interacting energies shown as dotted lines.

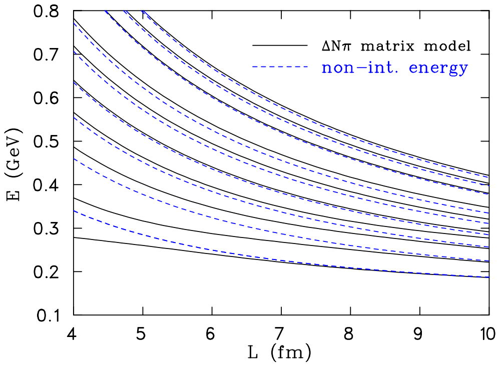

Lüscher's Method for Phase Shifts

- The finite-volume estimates of the phase shift δ, from Lüscher's formula:

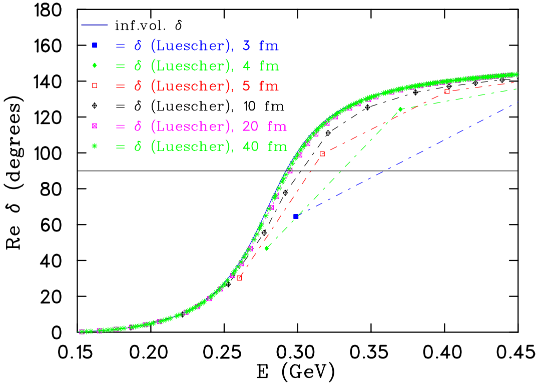

An Improved Method for Phase Shifts

- Clearly, the phase shifts from Lüscher's formula only converge very slowly to the infinite-volume phase shift.
- An improved method involves taking the Hamiltonian model, and constraining its free parameters (e.g. Δ_0, $g_{\Delta N}$ & Λ) using lattice data.
- These constrained parameters can be input into the t-matrix formula to obtain a phase shift more directly.

The Resonance Position at Finite Volume

- The resonance position ($\delta = 90^\circ$) can be plotted vs. $1/L$, comparing Lüscher's method and the improved method:

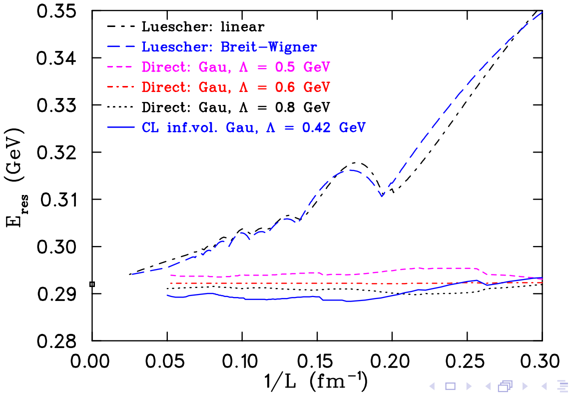

The Λ(1405)

- The negative-parity ground state of the Λ has a mass of $1405^{+1.3}_{-1.0}$ MeV.
- Such a low mass is puzzling:
  - Lies well below the positive-parity Λ(1600).
  - Lies lower than the N(1535), yet has a valence strange quark.

The $\Lambda(1405)$

- The negative-parity ground state of the Λ has a mass of $1405^{+1.3}_{-1.0}$ MeV.
- Such a low mass is puzzling:
  - Lies well below the positive-parity $\Lambda(1600)$.
  - Lies lower than the $N(1535)$, yet has a valence strange quark.

The Λ(1405)

- Our recent study has successfully isolated three low-lying states.

BJ Menadue *et al.*, Phys. Rev. Lett. **108**, 112001 (2012), arXiv:1109.6716

- The lowest state has a mass trend the reproduces the Λ(1405) in the physical limit.
- Extend this to investigate the electromagnetic structure of this unusual state.

Operator Choice

- There are a variety of interpolating operators that couple to the Λ baryon.
- We use the flavour-symmetry-specific operators

$$\chi_1^8 = \frac{1}{\sqrt{6}}\epsilon_{abc}(2(u_a^{\mathrm{T}}C\gamma_5 d_b)s_c + (u_a^{\mathrm{T}}C\gamma_5 s_b)d_c - (d_a^{\mathrm{T}}C\gamma_5 s_b)u_c)$$
$$\chi_2^8 = \frac{1}{\sqrt{6}}\epsilon_{abc}(2(u_a^{\mathrm{T}}Cd_b)\gamma_5 s_c + (u_a^{\mathrm{T}}Cs_b)\gamma_5 d_c - (d_a^{\mathrm{T}}Cs_b)\gamma_5 u_c)$$
$$\chi^1 = -2\epsilon_{abc}(-(u_a^{\mathrm{T}}C\gamma_5 d_b)s_c + (u_a^{\mathrm{T}}C\gamma_5 s_b)d_c - (d_a^{\mathrm{T}}C\gamma_5 s_b)u_c)$$

- We also use smearing at the source and sink (at 16 and 100 sweeps) to increase the operator basis.

Extracting Baryon Form Factors

- Given eigenstate-projected two- and three-point correlation functions G_α and G^μ_α, construct the ratio

$$R^\mu_\alpha(\Gamma_2, \Gamma_1; p', p; t_2, t_1) := \left(\frac{G^\mu_\alpha(\Gamma_1; p', p; t_2, t_1) G^\mu_\alpha(\Gamma_1; p, p'; t_2, t_1)}{G_\alpha(\Gamma_2; p'; t_2) G_\alpha(\Gamma_2; p; t_2)} \right)^{1/2} .$$

- We then define the reduced ratio

$$\overline{R}^\mu_\alpha := \left(\frac{2E_p}{E_p + M} \right)^{1/2} \left(\frac{2E_{p'}}{E_{p'} + M} \right)^{1/2} R^\mu_\alpha .$$

Extracting Baryon Form Factors

- A suitable choice of the spin projectors Γ_1 and Γ_2 now allows us to directly extract the Sachs form factors:

$$G_{\mathrm{E}}^{\alpha\pm}(Q^2) = \overline{R}_{\alpha}^{\mu}(\Gamma_4^{\pm}, \Gamma_4^{\pm}; q, 0, t_2, t_1),$$

$$|\varepsilon_{ijk} q^i| G_{\mathrm{M}}^{\alpha\pm}(Q^2) = (E_q + M)\overline{R}_{\alpha}^{\mu}(\Gamma_4^{\pm}, \Gamma_j^{\pm}; q, 0, t_2, t_1),$$

where the $\pm$ identifies the parity of the state α and

$$\Gamma_j^{+} = \frac{1}{2}\begin{bmatrix} \sigma_j & 0 \\ 0 & 0 \end{bmatrix}, \qquad \Gamma_4^{+} = \frac{1}{2}\begin{bmatrix} I & 0 \\ 0 & 0 \end{bmatrix}$$

$$\Gamma_j^{-} = \gamma_5 \Gamma_j^{+} \gamma_5 = \frac{1}{2}\begin{bmatrix} 0 & 0 \\ 0 & \sigma_j \end{bmatrix}, \qquad \Gamma_4^{-} = \gamma_5 \Gamma_4^{+} \gamma_5 = \frac{1}{2}\begin{bmatrix} 0 & 0 \\ 0 & I \end{bmatrix}$$

Electric Form Factor

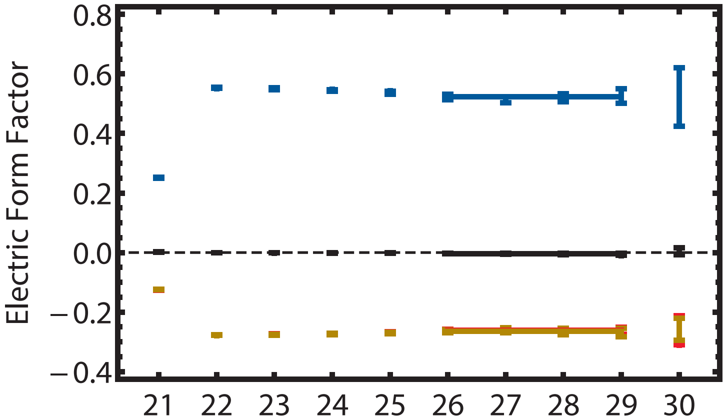

Electric Form Factor

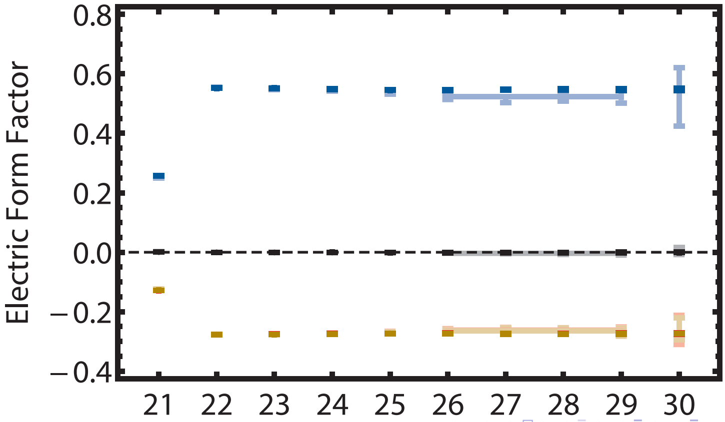

Electric Form Factor

sector	$\Lambda(1405)$	Λ
light	0.785(11)	0.8165(28)
strange	0.795(13)	0.8203(27)

Magnetic Form Factor

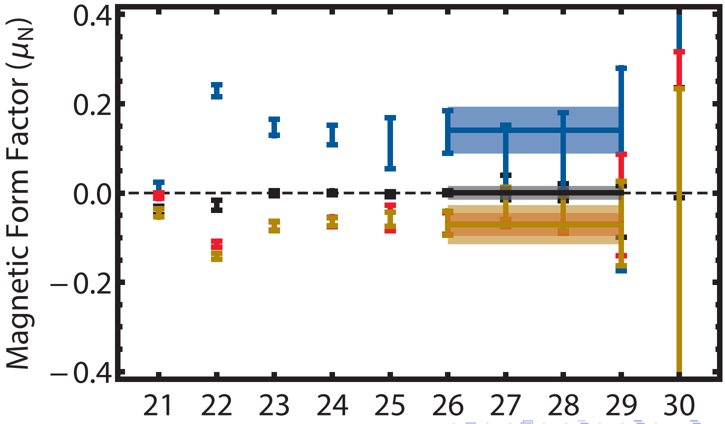

Magnetic Form Factor

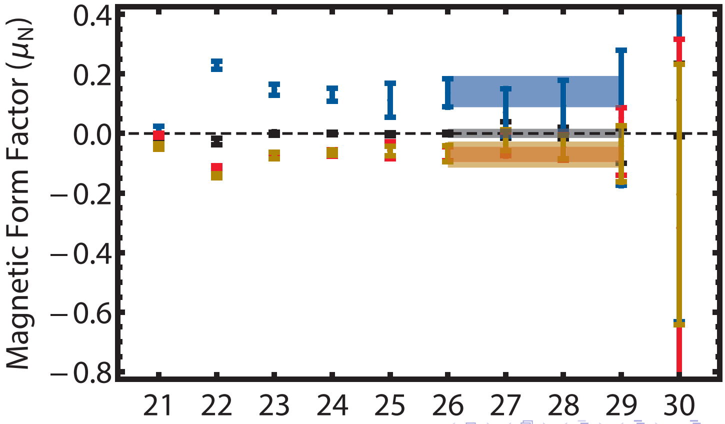

Magnetic Form Factor

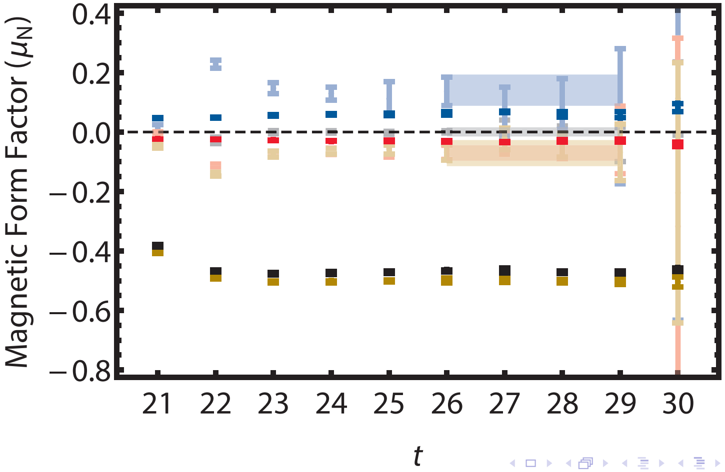

Magnetic Form Factor

sector	Λ(1405)	Λ
light	0.211(79)	0.0894(68)
strange	0.21(13)	1.493(12)

Values are in units of μ_N.

Charge Square Radii

sector	$\langle r_E^2 \rangle^{\Lambda(1405)}$	$\langle r_E^2 \rangle^{\Lambda}$	$\langle r_M^2 \rangle^{\Lambda(1405)}$	$\langle r_M^2 \rangle^{\Lambda}$
light	0.422(27)	0.3527(50)	0.224(66)	0.0591(38)
strange	0.399(32)	0.3442(84)	0.210(93)	0.959(20)

Values are in units of fm.

Magnetic Moment

sector	Λ(1405)	Λ
light	0.269(98)	0.1095(97)
strange	0.210(93)	1.820(15)

Values are in units of μ_N.

Summary

- Several fermion-source and -sink smearing levels have been used to construct correlation matrices.
- A variety of 4×4, 8×8 and 12×12 matrices have been considered to explore the eigenstate energies revealed by different interpolating field structures.
- The three-quark wave functions are reminiscent of early quark models.
- The approach of the Roper to the chiral limit is significantly different in quenched and full QCD.
  - An indication of significant mesonic dressings?

$N1/2^-$

- The $N1/2^-$ results in quenched and dynamical QCD reveal significant differences in the approach to the physical point.
- A level crossing between the Roper and $N1/2^-$ states is anticipated in full QCD at $m_\pi \simeq 150$ MeV, just above the physical pion mass.
- The approach to the experimentally measured masses in full QCD is encouraging.
- The effects of the finite volume on self-energy contributions and associated avoided level crossings remains to be resolved.

The $\Lambda(1405)$

- The mass trend of the lowest lying state is consistent with the physical $\Lambda(1405)$.
- The state can be accessed with a standard three-quark operator.
- It is predominantly flavour-singlet.
- The correlation-matrix analysis is vital to removing nearby excited-state contaminations.
- Currently examining the distribution of charge via electromagnetic form factors.

Hadron Spectrum Collaboration Results Comparison

- At the heaviest mass compared, we find the same number of N^+ states and qualitative agreement with the spectral energies.
- Finite-volume shifting of the P-wave $N\,\pi$ threshold is apparent in the spectra.
- Low-lying multi-particle states are suppressed on our large volume lattice for the three lightest quark masses.
- Qualitative agreement of the remaining N^+ states is manifest.
- Qualitative agreement is also observed for the lowest lying N^- states.
- Derivatives provided through the lower components of the Dirac spinors are sufficient to access the $N\frac{1}{2}^-$ spectrum.